Tonoplast cytochrome b561 is a transmembrane ascorbate-dependent monodehydroascorbate reductase: functional characterization of electron currents in plant vacuoles

New Phytologist

Tonoplast cytochrome b561 is a transmembrane ascorbate-dependent monodehydroascorbate reductase: functional characterisation of electron currents in plant vacuoles

Journal:	*New Phytologist*
Manuscript ID	NPH-MS-2022-41189.R1
Manuscript Type:	Full Paper
Date Submitted by the Author:	n/a
Key Words:	Electron currents, cytochrome b561, ascorbate, plant vacuole, anthocyanin

Complete List of Authors:

Gradogna, Antonella; CNR, Institute of Biophysics
Lagostena, Laura; CNR, Institute of Biophysics
Beltrami, Sara; University of Bologna, Department of Pharmacy and Biotechnology (FaBiT)
Tosato, Edoardo; University of Bologna, Department of Pharmacy and Biotechnology (FaBiT)
Picco, Cristiana; CNR, Institute of Biophysics
Scholz-Starke, Joachim; CNR, Institute of Biophysics
Sparla, Francesca; University of Bologna, Department of Pharmacy and Biotechnology (FaBiT)
Trost , Paolo; University of Bologna, Department of Pharmacy and Biotechnology (FaBiT)
Carpaneto, Armando; University of Genoa, Department of Earth, Environment and Life Sciences (DISTAV)

Tonoplast cytochrome b561 is a transmembrane ascorbate-dependent monodehydroascorbate reductase: functional characterisation of electron currents in plant vacuoles

Antonella Gradogna[1], Laura Lagostena[1], Sara Beltrami[2], Edoardo Tosato[2], Cristiana Picco[1], Joachim Scholz-Starke[1], Francesca Sparla[2], Paolo Trost[2]* and Armando Carpaneto[1,3]*

1. *Institute of Biophysics - CNR, Via De Marini 6, 16149 Genova, Italy*
2. *Department of Pharmacy and Biotechnology (FaBiT) - University of Bologna, Via Irnerio 42, 40126 Bologna, Italy*
3. *Department of Earth, Environment and Life Sciences (DISTAV) - University of Genoa, Viale Benedetto XV 5, 16132 Genova, Italy*

*Corresponding authors: Paolo Trost and Armando Carpaneto

Email: paolo.trost@unibo.it ; phone: +390512091329; fax: +39051242576 ;

Email: armando.carpaneto@unige.it ; phone: +390103538570; fax: +39010352169.

Key words

Electron currents, cytochrome *b*561, ascorbate, plant vacuole, anthocyanin

Abstract

- Ascorbate (Asc) is a major redox buffer of plant cells, whose antioxidant activity depends on the ratio with its one-electron oxidation product monodehydroascorbate (MDHA). The cytoplasm contains millimolar concentrations of Asc and soluble enzymes that can regenerate Asc from MDHA or fully oxidized dehydroascorbate. Also vacuoles contain Asc, but no soluble Asc-regenerating enzymes.
- Here we show that vacuoles isolated from Arabidopsis mesophyll cells contain a tonoplast electron transport system that works as a reversible, Asc-dependent transmembrane MDHA oxidoreductase.
- Electron currents were measured by patch-clamp on isolated vacuoles and found to depend on the availability of Asc (electron donor) and ferricyanide or MDHA (electron acceptors) on opposite sides of the tonoplast.
- Electron currents were catalyzed by cytochrome b561 isoform A (CYB561A), a tonoplast redox protein with cytoplasmic and luminal Asc binding sites. The K_m for Asc of the luminal (4.5 mM) and cytoplasmic site (51 mM) reflected the physiological Asc concentrations in these compartments. The maximal current amplitude was similar in both directions.
- Mutant plants with impaired CYB561A expression showed no detectable trans-tonoplast electron currents and strong accumulation of leaf anthocyanins under excessive illumination, suggesting a redox-modulation exerted by CYB561A on the typical anthocyanin response to high-light stress.

Introduction

Ascorbate (Asc) is a versatile antioxidant of plant cells that can reduce non-enzymatically different types of radicals and transition metals, and serve as a substrate of several enzymes including Asc peroxidase, Asc oxidase (Foyer *et al.*, 2020) and cytochrome *b*-561 (CYB561) (Asard *et al.*, 2013). Asc is also a cofactor for 2-oxoglutarate-dependent dioxygenases whose catalytic iron is maintained in the reduced/active state by Asc (Smirnoff, 2018). Non-enzymatically, Asc can also reduce protein

sulfenic acids thereby potentially interfering with thiol-based redox regulatory systems (Zaffagnini *et al.*, 2019; Anschau *et al.*, 2020). In all redox reactions in which it is involved, Asc donates a hydrogen atom (one electron and one proton) and is converted to monodehydroascorbate (MDHA; Njus *et al.*, 2020). As a radical, MDHA is relatively stable but can be reduced back to Asc by NADH-monodehydroascorbate reductase (MDHAR; Hossain & Asada, 1985; Park *et al.*, 2016) or ferredoxin (Foyer *et al.*, 2020), or react with other radicals, including itself (Njus *et al.*, 2020). Spontaneous disproportionation of MDHA radicals gives rise to Asc and fully oxidized dehydroascorbate (DHA) that is chemically unstable. DHA can be reconverted to Asc by glutathione-dependent DHA reductase (DHAR) or alternative systems relying on different electron sources (Potters *et al.*, 2004; Terai *et al.*, 2020). All these reactions and properties are relevant for the current study dealing with an Asc-dependent MDHA oxidoreductase activity that connects cytoplasmic and vacuolar Asc pools across the tonoplast membrane.

The concentration of Asc in plant cells is generally very high. In leaves, compartments such as the cytosol, chloroplast stroma, mitochondria and peroxisomes contain Asc in the order of tens of millimolar (Heyneke *et al.*, 2013; Zechmann, 2018; Foyer *et al.*, 2020). These compartments are characterized by neutral pH and contain NADH-dependent MDHARs that regenerate Asc from MDHA, but also Asc peroxidases that convert Asc to MDHA in the presence of H_2O_2 (Noctor *et al.*, 2018; Smith *et al.*, 2021). Although the *in vivo* determination of MDHA is impractical, the combined effects of MDHA spontaneous dismutation and MDHAR activity are believed to keep MDHA at very low levels in these cell compartments (Smirnoff, 2018). Indeed, a high local Asc/MDHA ratio is what makes Asc a good reductant *in vivo*, in spite of its very positive standard redox potential ($E°'_{Asc/MDHA}$ +280 mV) (Njus *et al.*, 2020). Differently from Asc/MDHA, Asc/DHA ratios are routinely measured in leaf extracts and values found are typically above 10, but most of the DHA is likely to derive from the apoplast (Noctor, 2006). Anyway, DHA as such does not directly influence the antioxidant properties of Asc, that essentially depend on the Asc/MDHA ratio and on pH.

Acidic compartments of plant cells, like the apoplast and the vacuole, do also contain Asc but lack MDHARs and DHARs (Noctor & Foyer, 2016; Smirnoff, 2018). In the apoplast, the concentration of Asc is in the millimolar range (Zechmann, 2018) and typically lower than DHA (Foyer *et al.*, 2020). The apoplast is also the site where Asc can be oxidized by Asc oxidase and DHA degraded by specific pathways (Smirnoff, 2018; Foyer *et al.*, 2020).

In the vacuole, Asc concentration is also millimolar but the Asc/DHA ratio can be higher than in the apoplast (Ferreres *et al.*, 2011). Since most living plant cells contain a large central vacuole that can occupy more than 80% of the cellular volume (Shitan & Yazaki, 2020), the vacuolar pool of Asc can be as large as the cytosolic pool in a typical photosynthetic plant cell (Zechmann, 2018). Vacuoles neither contain Asc oxidase nor other soluble enzymes that specifically use Asc as a reductant, but contain phenolic compounds, including anthocyanins that can reduce hydrogen peroxide either chemically (Csepregi & Hideg, 2018) or enzymatically via membrane bound class III peroxidases (Ferreres *et al.*, 2011; Zipor *et al.*, 2015; Lüthje & Martinez-Cortes, 2018; Smirnoff & Arnaud, 2019). In both cases anthocyanin oxidation generates phenoxy radicals which can rapidly oxidize Asc to MDHA, and MDHA to DHA (Takahama, 2004; Ferreres *et al.*, 2011; Smirnoff & Arnaud, 2019). In leaves, the biosynthesis of both Asc and anthocyanins is strongly stimulated under excessive illumination, the same conditions that drive the production of hydrogen peroxide by photosystem I (Foyer *et al.*, 2020). However, besides the antioxidant function that connects anthocyanins with Asc, anthocyanins play also a photoprotective role, independently from Asc, based on the efficient absorption of green and yellow components of the photosynthetically active radiation (Zheng *et al.*, 2021).

Asc is synthesized in the cytosol, with the last enzyme of the pathway being associated to the internal membrane of mitochondria (Smirnoff, 2018). How Asc is distributed in different cell compartments is little known. An intracellular Asc transporter is known to be located on the inner membrane of chloroplasts (Miyaji *et al.*, 2015) and a member of the multidrug and toxic compound extrusion family that works as an ascorbate/proton antiporter (AtDTX25; Hoang *et al.*, 2021) was recently described

in the vacuolar membrane of Arabidopsis. The vacuolar Asc transporter AtDTX25, is highly expressed in seedlings where it promotes the reduction and mobilization of Fe^{3+} stored in vacuoles. AtDTX25 is also expressed in flowers, with still unknown function, but not in leaves (Hoang *et al.*, 2021). On the other hand, vacuoles isolated from barley leaves were shown to slowly uptake DHA and Asc following the concentration gradient, with no evidence for any detectable transport system (Rautenkranz *et al.*, 1994).

The tonoplast membrane of species like *Arabidopsis thaliana* and *Phaseolus vulgaris* also contains at least one member of the cytochrome b561 family of di-heme proteins that, as a general property, catalyze transmembrane electron transports using Asc as electron donor and MDHA or metal compounds as electron acceptors (Asard *et al.*, 2013). Arabidopsis contains four CYB561 orthologues and several related cytochromes in which CYB561 domains are combined with one or more extracellular DOMON domains, each binding an additional heme (CYBDOM; Preger *et al.*, 2005; Tsubaki *et al.*, 2005; Asard *et al.*, 2013). One CYBDOM isoform was experimentally localized on the plasma membrane (Picco *et al.*, 2015). Among CYB561s (also known as CYBASC for Asc-reducible cytochromes b; Preger *et al.*, 2005; Klein *et al.*, 2020), the isoform A (CYB561A) was localized on the tonoplast in Arabidopsis leaves (Griesen *et al.*, 2004) and in etiolated bean hypocotyls (Preger *et al.*, 2005), but on the plasma membrane in wild watermelon (*Citrullus lanatus*; Nanasato *et al.*, 2005). The intracellular location of the remaining three CYB561 isoforms (B-D) is unknown but the crystal structure of CYB561B from *Arabidopsis thaliana* was solved (Lu *et al.*, 2014). Arabidopsis CYB561B is a homodimer and each monomer is made of six transmembrane α-helices with two heme groups coordinated by two histidine pairs. In each monomer, two cavities, each located in close proximity to a heme and facing different sides of the membrane, are the Asc binding sites (Lu *et al.*, 2014). Tonoplast CYB561A is predicted to share with CYB561B of Arabidopsis and other CYB561 members of the family the same overall structure (Asard *et al.*, 2013; Lu *et al.*, 2014; Ganasen *et al.*, 2018). The residues involved in heme coordination and Asc binding are also largely conserved among plant and animal CYB561 orthologues (Lu *et al.*, 2014).

In this work we show that CYB561A catalyzes a trans-membrane electron transport from Asc on one side of the tonoplast membrane to MDHA or an artificial electron acceptor like ferricyanide on the other side of the membrane. Electron currents, detected 38 years after the first patch-clamp potassium current recordings in plant cells (Moran *et al.*, 1984; Schroeder *et al.*, 1984), are reversible and can be measured by whole-vacuole patch clamp experiments with vacuoles isolated from mesophyll Arabidopsis protoplasts. Steady state kinetic analyses allowed to determine kinetic parameters associated to each of the two Asc binding sites, indicating the role that CYB561A may play in connecting the redox states of different Asc pools separated by the tonoplast membrane. CYB561A appears to be the major protein responsible for the Asc-dependent electron transport detected in Arabidopsis vacuoles and plants with lower expression of the *CYB561A* gene are shown to over-accumulate anthocyanins in response to high light, pinpointing a plausible redox role played by CYB561A in modulating this photoprotective response.

Results

Cytosolic ascorbate and vacuolar ferricyanide elicit cytosol-to-lumen directed electron currents in Arabidopsis vacuoles

With the aim of testing whether a trans-tonoplast electron transport could be detected *ex vivo*, whole-vacuole patch-clamp experiments were performed on intact vacuoles isolated from *Arabidopsis thaliana* mesophyll protoplasts. Prolonged whole-vacuole patch-clamp recordings were carried out at 0 mV, a tonoplast voltage in the physiological range (-30 to 0 mV) (Bethmann *et al.*, 1995; Walker *et al.*, 1996; Hedrich, 2012). Addition of 10 mM Asc to the bath medium corresponding to the cytosolic side of the vacuole, did not elicit any trans-membrane current. Clear inward currents were instead elicited when the vacuolar lumen was pre-equilibrated with a generic electron acceptor like ferricyanide (FeCN; 1 mM). The effect was reversible and the current returned to the basal level upon Asc wash-out (Fig. 1a).

In principle, the observed inward currents could result from an electron transport system connecting cytosolic Asc to luminal FeCN, or alternatively from the activation of ion fluxes, either anions moving into the vacuole or cations moving from the vacuole to the cytosol. The currents observed in the presence of cytosolic Asc and vacuolar FeCN, however, were not affected by substituting the major ions of the bath solution (K^+, Cl^-) with large, membrane impermeable charged molecules (BTP^+, MES^-). This indicated that potassium and chloride were not involved in the Asc/FeCN-dependent currents (Fig. 1b). Moreover, Asc/FeCN-dependent currents were not affected by a vacuolar pH shift from 5.5 to 6.5 (Fig. 1b) suggesting that proton-coupled transport activities were not involved. The apparent insensitivity to the vacuolar pH was thus consistent with an electron transport activity resulting in the reduction of luminal ferricyanide (FeCN), considering that no protons are involved in the reduction of ferri to ferrocyanide ($[Fe^{3+}(CN)^-_6]^{3-}$ + 1 e^- -> $[Fe^{2+}(CN)^-_6]^{4-}$). Cytosolic Asc to luminal FeCN electron currents were measured at different membrane potentials and were active at physiological voltages (Suppl. Fig.1). In eliciting the electron transfer to FeCN, Asc could not be substituted by a different electron donor like dithiothreitol (DTT) (Fig. 1cd). Overall, these results are fully consistent with Asc-evoked currents mediated by an electron transport system that connects cytosolic Asc to luminal FeCN, and exclude concomitant ion transports.

Currents could be further characterized by varying the concentration of Asc in the bath (cytosolic) solution, at different concentrations of FeCN in the vacuole. All experiments were performed at 0 mV and absence of proton gradient (pH 7.5 in both cytosol and lumen). Current densities, i.e. currents divided by the capacitance of the vacuole, were used to compare data obtained from vacuoles of different sizes. For the sake of simplicity, we will use the term current instead of current density throughout the text. Fig. 2ad shows that currents increased in amplitude in both Asc- and FeCN-dependent manner. The apparent kinetic parameters, i.e. the apparent Michaelis-Menten constants for cytosolic Asc (K_{Ac}^{app}) and vacuolar FeCN (K_{Fv}^{app}) and the maximal currents interpolated at saturating Asc (I_{Acmax}^{app}) or FeCN concentrations (I_{Fvmax}^{app}) allowed estimating the limiting kinetic parameters by secondary plots (Fig. 2bcef). Continuous lines in Fig. 2bcef are obtained by a global fitting procedure using an extended Michaelis-Menten equation (see Mathematical model in

Methods). In this way the electron transport system is kinetically described as a trans-tonoplast oxidoreductase with a K_m for cytosolic Asc (K_{Ac}) of 51±8 mM, a K_m for vacuolar FeCN (K_{Fv}) of 1.0±0.2 mM and a maximal electron transport capacity (I_{cvmax}) of 3.7±0.5 pA/pF (Table 1).

Vacuolar ascorbate and cytosolic FeCN elicited lumen-to-cytosol directed electron currents in Arabidopsis vacuoles

The reversibility of the electron transport system was tested by loading the vacuole with 5 mM Asc and adding 100 µM FeCN to the bath medium, as shown in Fig. 3. In this inverted configuration, the application of cytosolic FeCN evoked outward currents that disappeared upon FeCN wash-out (Fig. 3a, middle trace). In contrast, FeCN did not alter the currents in control vacuolar solution (without Asc, Fig. 3a, top trace) or when Asc was substituted by DTT (Fig. 3a, bottom trace).

The combined results of Fig. 1 and Fig. 3 clearly showed that Asc oxidation, and symmetrically FeCN reduction, could occur on both sides of the vacuolar membrane. When the electron donor Asc was in the vacuole, and the electron acceptor FeCN was cytosolic, outward currents were thus compatible with a vacuole-to-cytosol electron transport. Influence of the membrane potential was again measured during a series of voltage pulses ranging from -60 to 60 mV. The electron transport was active at physiological tonoplast voltages (Suppl. Fig. 2)..

Dose-response experiments were performed at 0 mV and 0 ΔpH to estimate the dependence of electron currents on vacuolar Asc and cytosolic FeCN concentrations. Patch-clamp experiments were carried out with different Asc concentrations in the pipette (1 to 40 mM, vacuole) and different FeCN concentrations in the bath solution (3.3 to 100 µM, cytosol). Positive currents normalized to membrane capacitance (i.e. current density), increased at increasing concentrations of either FeCN or Asc. Current amplitudes (Fig. 4a) were plotted as a function of the varied substrate (Fig. 4be). Data fitting by parametric hyperbolae returned the apparent Michaelis-Menten constants for both

vacuolar Asc (K_{Av}^{app}) and cytosolic FeCN (K_{Fc}^{app}), and the maximal currents interpolated at saturating Asc (I_{Avmax}^{app}) or FeCN concentrations (I_{Fcmax}^{app}). Limiting kinetic parameters were obtained following the same procedure of Fig. 2 (Figure 4cdfg). Limiting K_m values for vacuolar Asc (K_{Avac}) and cytosolic FeCN (K_{Fcyt}) were 4.5±1.0 mM and 24±2 μM, respectively, with the maximal current (I_{vcmax}) being 3.1±0.9 pA/pF (Table 1). The oxidoreductase system transferring electrons from ascorbate to ferricyanide across the tonoplast is thus fully reversible and has similar maximal electron current capacities in either direction, though kinetic affinities for the substrates on either side of the membrane are very different (Table 1).

Detecting the vacuolar acidification associated to ascorbate oxidation

The trans-tonoplast electron transport so far characterized relies on the presence of an electron donor (Asc) and an electron acceptor (FeCN) on opposite sides of the membrane. The first step of this process is expected to involve a one-electron oxidation of Asc to MDHA with concomitant release of one proton in the medium ($Asc^- \rightarrow MDHA^- + 1e^- + 1\ H^+$). Whether Asc oxidation was associated to a detectable pH change was investigated with the ratiometric fluorescent pH indicator 2',7'-bis-(2-carboxyethyl)-5-(and-6)-carboxyfluorescein (BCECF) that was loaded in the lumen of the vacuole from the patch pipette. Whole-vacuole patch-clamp experiments were performed with 5 mM Asc and 10 μM BCECF in the vacuole upon increase of cytosolic FeCN concentrations. Conversion of BCECF fluorescence ratios (490/440 nm) into pH values was based on a pH calibration procedure previously described (Carpaneto *et al.*, 2017; Gradogna *et al.*, 2021). Positive currents were recorded simultaneously with the BCECF fluorescence ratio, at a holding potential of 0 mV (Fig. 5a). Interestingly, currents increased with increasing cytosolic FeCN and nicely matched with the reversible increase of vacuolar lumen acidification (Fig. 5ab). In the absence of Asc in the pipette, only a slight acidification was observed at the highest concentration of cytosolic FeCN (100 μM) (Fig. 5b). Results are hence consistent with vacuolar Asc being the source of both electrons for cytosolic FeCN reduction and protons for luminal acidification.

Ascorbate-dependent trans-tonoplast electron currents detected in isolated vacuoles of Arabidopsis mesophyll protoplasts depend on cytochrome b561 isoform A (CYB561A)

The Asc-dependent, trans-tonoplast electron transport characterized so far is compatible with the activity of cytochrome b-561, possibly cytochrome b561 isoform A (CYB561A) previously associated to vacuolar (Preger *et al.*, 2005) or plasma membranes (Nanasato *et al.*, 2005) in different plant species including Arabidopsis (Griesen *et al.*, 2004). The targeting of Arabidopsis CYB561A to the tonoplast was confirmed here by the confocal analysis of Arabidopsis protoplasts transformed with a CYB561A-EGFP construct (Suppl. Fig. 3).

Two homozygous T-DNA insertional lines for At4g25570 were isolated. Line *cyb561a-1* carries an insertion in the first intron while line *cyb561a-2* shows an insertion in the third exon of the *CYB561A* gene. The level of *CYB561A* transcripts was analysed in rosette leaves and found to be much lower, albeit not absent, in both mutant lines in respect to wild type (Suppl. Fig. 4).

Whole-vacuole patch-clamp experiments were performed on vacuoles isolated from either mutant line. Addition of 10 mM cytosolic Asc in the presence of 1 mM vacuolar FeCN did not yield to any detectable inward current (Fig. 6ab). Symmetrically, addition of 100 µM cytosolic FeCN in the presence of 5 mM vacuolar Asc did not induce any detectable outward current (Fig. 6cd) or vacuolar acidification (Suppl. Fig. 5). CYB561A is thus concluded to be the responsible for the bi-directional Asc-to-FeCN electron transport detected in isolated vacuoles.

CYB561A mediates electron transport from vacuolar ascorbate to cytosolic monodehydroascorbate

Given the high structural similarity between Asc and its oxidation product MDHA, CYB561A is expected to bind also MDHA in both its Asc binding sites. Once bound, MDHA could act as an electron acceptor as shown for cytochromes b561 *in vitro* (Nakanishi *et al.*, 2009; Bérczi & Zimányi,

2014). Here we tested whether the electron transport from luminal Asc to cytosolic MDHA could also be detected in isolated vacuoles.

To this aim, Asc was included in the luminal pipette solution and the vacuole was perfused with an ionic solution containing Asc oxidase (AO-solution). The AO-solution was then changed with an ionic solution containing Asc (Asc-solution) (Figure 7a). At the interface between the two solutions, AO interacts with Asc and generates MDHA that should locally reach a finite concentration before dismutating to Asc and DHA. In the perfusing chamber, freshly produced MDHA could possibly act as an electron acceptor for CYB561A, itself reduced by Asc from the inside of the vacuole. Indeed, positive currents were clearly elicited when the solution interface entered into the perfusing chamber and bathed the vacuole. The current was transient as long as the Asc/AO solution was washed out by the perfusing flow (Figure 7ab). Electron currents were again completely abolished in vacuoles isolated from both *cyb561a* mutant lines (Figure 7bc).

In wild type vacuoles, electron currents could be modulated by varying the concentration of Asc used by AO to generate MDHA. Variations were observed in the sub-millimolar range (0.03-1 mM) according with the K_m for Asc of AO (0.2 mM; Wimalasena & Dharmasena, 1994) (Fig. 7d). At Asc concentrations higher than 1 mM, AO was saturated and so was the electron current stimulation. Interestingly, Asc concentrations up to 20 mM did not compete with the capability of MDHA to bind the cytosolic site of CYB561A and act as electron acceptor (Fig. 7d), a result that is consistent with the high K_m for Asc of the cytosolic site of CYB561A (51 mM; Table 1).

The electron currents generated by Asc/AO were voltage-dependent as shown by voltage ramps (Suppl. Fig. 6). Currents were enhanced by positive cytosolic voltages which would actually facilitate the movement of electrons from vacuolar Asc to cytosolic MDHA; again, similar to all other conditions investigated in this study (Suppl. Fig. 1 and 2), the trans-tonoplast electron transport is active at physiological tonoplast voltages between -30 and 0 mV. The same experiments performed with vacuoles isolated from the two *cyb561a* mutant lines gave no response, strongly suggesting that

MDHA was the cytosolic acceptor of electrons which moved from vacuolar Asc and crossed the vacuolar membrane by means of CYB561A.

CYB561A mutant plants show an exaggerated response to high light in terms of anthocyanin accumulation in leaves

Mutants of *CYB561A* were analysed for Asc content in total leaf extracts from 14-day plants grown on agar plates under standard illumination (100 μE m^{-2} s^{-1}). Compared to wild type plants, Asc and Asc+DHA were slightly higher in one of the two mutant lines (*cyb561a-2*) (Fig. 8a), although the Asc/(Asc+DHA) ratio was similar in all genotypes (0.89 on average with no significant differences among genotypes; Suppl. Fig. 7). Nitroblue tetrazolium (NBT) reactive compounds, which are expected to be inversely related to Asc, were lower in both mutant lines with respect to wild type plants (Fig. 8b).

In mature 7-week old plants, the small differences in Asc content observed in young plants were not apparent anymore (Fig. 8c, control). Neither Asc levels nor Asc/(Asc+DHA) ratios were significantly different in leaves of the three genotypes grown under standard light intensity (100 μE m^{-2} s^{-1}). As a typical response of mature plants to excessive illumination, Asc content increased in both wild type and mutants during a prolonged high light treatment (HL; 700 μE m^{-2} s^{-1}). At the end of HL experiments (11 days), leaf Asc content was similarly increased in all genotypes (from 4.3-fold in wild type to 5.3-fold in *cyb561a-1*; Fig. 8c). The Asc/(Asc+DHA) ratio was unaffected by the HL treatment throughout the experiment (0.96 on average with no significant differences among genotypes and time points; Suppl. Fig. 7).

Rosette leaves of all genotypes contained no detectable anthocyanins under standard illumination but turned purple because of anthocyanin accumulation during the HL treatment (Suppl. Fig. 8). In wild type plants, anthocyanins were detected at constant levels starting from day 4 of strong illumination. In mutant lines the response was amplified and anthocyanin concentration in mutant

leaves exceeded that of wild type by a factor of 2.1-2.7 at day 4, and by a factor of 4.5-4.6 at the end of the treatment (Fig. 8d). The overaccumulation of anthocyanins under HL was overall the most clear and quantifiable phenotypic effect of the diminished *CYB561A* expression in Arabidopsis mutants.

Discussion

Isolated vacuoles of Arabidopsis leaves are here shown to possess an electron transport system that is able to transfer electrons from cytosolic Asc to a soluble electron acceptor inside the vacuole and vice versa. The electron acceptor can be FeCN, an artificial and stable compound that is reduced to the stable product ferrocyanide, or MDHA, a physiological short living radical produced by Asc oxidation. MDHA reduction by the electron transport system gives rise to Asc again on the other side of the membrane. Overall, the activity of the electron transport system can be defined as trans-tonoplast, Asc-dependent MDHA oxidoreductase and here is shown to depend on cytochrome b561 isoform A (CYB561A). Among the four CYB561s of Arabidopsis, CYB561A appears to be the only functional isoform in vacuoles of mesophyll cells or at least, the only one whose activity could be electrophysiologically detected under tested conditions. Currents were in fact undetectable in mutants with strongly reduced expression of the *CYB561A* gene.

Studying the activity of an electron transporter like CYB561A in intact vacuoles with patch-clamp has several advantages. With this technique, the electron transport activity is detected with the protein inserted in its native lipid environment, with the membrane bilayer separating the two aqueous compartments in which the substrates are dissolved. Moreover, the tonoplast voltage is fixed. This condition allows measuring transmembrane currents evoked by any chosen combination of electron donors and acceptors, present on opposite sides of the membrane. This is essential for proteins like CYB561s with two active sites for Asc that are separated by the membrane in native conditions, but freely accessible from the medium in *in vitro* studies performed with the purified protein kept in a soluble state by interacting detergents.

By measuring the electron transport activity catalysed by CYB561A in intact vacuoles we could perform steady-state kinetic analyses and derive all kinetic parameters required to define the kinetic model, i.e. the maximal electron transport activity in either direction (I_{cvmax}, I_{vcmax}) and the K_m for Asc and FeCN for both cytosolic and luminal binding sites (K_{Ac}, K_{Fv}, K_{Av}, K_{Fc}). The maximal rates of

366 electron transport (I_{max}) that CYB561A can catalyse in the two directions are similar, suggesting that
367 the energy barriers the electrons have to overcome to travel from the cytosol to the vacuole and vice
368 versa are symmetric. Double reciprocal plots of the primary kinetic data show parallel patterns
369 consistent with a ping pong reaction mechanism and a simple equation to model the activity of
370 CYB561A at any given concentration of electron donor and acceptor could be derived, see Methods
371 and (Picco *et al.*, 2014).
372
373 Our measures allowed an unprecedented determination of specific K_m values for CYB561A
374 substrates, with the cytoplasmic site showing higher K_m values for both Asc and FeCN in respect to
375 the luminal site (Table 1). Interestingly, in the case of Asc as the physiological electron donor, the
376 cytoplasmic and luminal K_m values (51 and 4.5 mM, respectively) are well suited to the cytosolic and
377 luminal concentrations of Asc determined by quantitative immunoelectron microscopy in mesophyll
378 Arabidopsis cells (22 mM and 2 mM, respectively; Zechmann, 2018), thereby further supporting a
379 bidirectional electron transport system.
380
381 The prevalent direction of the electron transport catalysed by CYB561A *in vivo* depends in theory on
382 the difference in redox potential of the Asc/MDHA couple between cytoplasm and vacuole. Where
383 the redox potential is lower, Asc acts as an electron donor; where the potential is higher, MDHA is
384 the electron acceptor. This condition sets the net direction of the electron transfer. The difference in
385 redox potential depends on Asc/MDHA ratios and on ΔpH, because one proton is involved in the
386 reaction (MDHA+ $1e^-$ + $1H^+$→ Asc). Unfortunately, the intracellular concentration of MDHA, and
387 hence the redox potential of Asc, is unknown and is likely to remain so until a genetically coded, Asc-
388 specific biosensor will be available. The effect of pH is also difficult to predict because on one side
389 the low pH of the lumen favours MDHA reduction by CYB561A, but on the other it speeds up MDHA
390 dismutation (MDHA + MDHA + $1H^+$ → Asc + DHA) which is also pH-dependent and produces DHA
391 besides Asc, thus lowering the total concentration of Asc in compartments like the vacuole that lack
392 DHAR activities. So, no strong predictions on the prevailing direction of CYB561 activity can be made
393 based on solid available data.

In spite of this lack of knowledge, it is widely accepted that cytochromes b561 are redox systems that both in animals and plants transfer electrons from cytoplasmic Asc to extracytoplasmic MDHA (or alternative electron acceptors as iron chelates; Asard *et al.*, 2013). The main reason supporting this view is that the cytoplasm is a compartment where Asc is kept reduced by MDHARs and DHARs, while extra-cytoplasmic compartments like the vacuole or the apoplast do not contain these activities and therefore may require the MDHA reductase activity of CYB561.

Vacuoles do not contain enzymes that oxidize Asc directly, but phenolic compounds that may form phenoxy radicals by reacting with H_2O_2 (Csepregi & Hideg, 2018), directly or enzymatically via vacuolar class III peroxidases (Takahama, 2004; Ferreres *et al.*, 2011; Smirnoff, 2018). Phenolic compounds include anthocyanins that, together with Asc, are increasingly accumulated in vacuoles under conditions of excessive illumination that concomitantly leads to H_2O_2 production (Zipor *et al.*, 2015; Zechmann, 2018; Smirnoff & Arnaud, 2019; Zheng *et al.*, 2021). Since Asc is a good reductant of phenoxy radicals (Takahama, 2004; Smirnoff, 2018), CYB561A may be a system to restore the redox state of vacuolar Asc at the expense of cytosolic Asc under high light conditions. This hypothesis reminds a similar hypothesis put forward to explain the role of CYB561 in *Citrullus lanatus* in high light, provided that in this species CYB561 is localized on the plasma membrane and is coexpressed with apoplastic Asc oxidase under HL stress (Nanasato *et al.*, 2005; Foyer *et al.*, 2020).

The phenotypic analysis of CYB561A mutants provides new insights into the inter-relationship between Asc and anthocyanin in HL conditions. Mutants with diminished expression of *CYB561A* show similar Asc levels and similar Asc redox state (Asc/(Asc+DHA)) as wild type plants, but accumulate many more anthocyanins in high light conditions. The lack of control exerted by CYB561A on Asc levels of whole leaf extracts is not surprising since CYB561A may symmetrically control the redox states of cytosolic and vacuolar Asc without changing its total concentration nor its redox state in whole cells. A positive correlation between Asc and anthocyanins in HL was already observed in different Arabidopsis ecotypes and Asc biosynthetic mutants (Page *et al.*, 2012; Plumb

et al., 2018) and explained by the positive effect of Asc on the expression of several anthocyanin biosynthetic genes and transcription factors that control the pathway (Munné-Bosch & Müller, 2013; Smirnoff, 2018). In this framework, the over accumulation of anthocyanins induced by HL in plants with diminished *CYB561A* expression might be related to altered Asc levels or redox states in specific subcellular compartments that still need to be investigated.

In conclusion, here we show that it is possible to record electron currents in plant vacuoles by applying the patch-clamp technique and that CYB561A represents a redox connection between the cytoplasmic and the vacuolar pools of Asc in Arabidopsis mesophyll cells. Under conditions in which vacuolar Asc is oxidized to MDHA, CYB561A can regenerate it by oxidizing cytoplasmic Asc. The reverse reaction is also possible and fully sustained by kinetic parameters, determined here for the first time with an electrophysiological approach. Mutants with lower *CYB561A* expression have no altered Asc levels in total leaf extracts, but overaccumulate leaf anthocyanins under prolonged high light stress, suggesting a new unexplored connection between anthocyanin biosynthesis and an Asc-dependent electron transport system of the tonoplast.

Methods

Selection of homozygous insertional mutants of Arabidopsis thaliana

Stock seeds of two independent CYB561-A (At4g25570) T-DNA lines were purchased from the European Arabidopsis Stock Center (NASC, Nottingham, U.K.). Five plants from each line were analysed by PCR for homozygous selection. Two independent PCR amplifications were performed on genomic DNA extracted from leaves. The two pairs of primers for SALK_069822 (cytb561-a1) were cyb561-a1 fw (5'- AATAGTTTCCATTGCGCAATG-3') plus cyb561-a1 rev (5'-TCAGAACACAAACACAGACGG-3') and cyb561-a1 rev plus LBb1.3 (5'-ATTTTGCCGATTTCGGAAC-3'). The two pairs of primers for SALK_058385C (cytb561-a2) were cyb561-a2 fw (5'- CACACCAGAAGTAGCAAAGCC-3') plus cyb561-a2 rev (5'-TTGTGTTACCAAAGCAAAGGG-3') and cyb561-a2 rev plus LBb1.3. A Biometra T-gradient thermocycler was used for PCR amplifications with the following parameters: 5 min at 94 °C followed by 35 cycles of 30 s at 93 °C, 30 s at 58 °C and 1 min at 72 °C. PCR products were analysed on 0.8% (w/v) agarose gel in TAE buffer and visualized with GelRed (Suppl. Fig. 4).

Homozygous T-DNA lines were checked for residual expression level of the gene At4g25570; three independent total RNA extractions were performed on wild type and T-DNA adult plants using Spectrum™ Plant Total RNA Kit (Merck). Reverse transcription was performed on 1 µg of total RNA using OneScript® Plus cDNA Synthesis Kit (abm®) with Oligo(dT) primer. *CYB561-A* specific PCR-primers were CYB561-A fw 5'-TCCTGGATTGGTATTGGAGT-3' and CYB561-A rev 5'-ATGCTTCGGATCCATACTTG-3' and PCR amplification was performed using the following conditions: 30 s at 95 °C followed by 30 cycles of 30 s at 95 °C, 30 s at 48 °C and 20 s at 68 °C and a final extension at 68 °C for 5 min. As control the expression level of the gene *ACT8* (At1g49240) was used. The following pair of primers ACT8 fw 5'- CTCAGGTATTGCAGACCGTATGAG-3' and ACT8 rev 5'- CTGGACCTGCTTCATCATACTCTG-3' was used and the following amplification conditions were applied: 30 s at 95 °C followed by 30 cycles of 30 s at 95 °C, 30 s at 53 °C and 20 s at 68 °C and ending with 5 min at 68 °C.

After amplification, the amount of PCR products was visualized using 1% (w/v) agarose gel electrophoresis with GelRed and analysed by ImageJ (Suppl. Fig. 4).

467

468 *Plant growth conditions*

469 *Arabidopsis thaliana* plants, both wild type and mutants, were grown on soil at 22 °C, under 12/12 h
470 light/dark cycle with a photosynthetic photon flux density of 100 µmol m^{-2} sec^{-1}.
471 Stress condition was imposed by transferring 48-day old plants to high light (HL; photosynthetic
472 photon flux density of 700 µmol m^{-2} sec^{-1}). Plants were collected after 4, 7 and 11 days of HL
473 treatment (52-, 55- and 59-day old plants, respectively). Both control and treated samples were
474 immediately frozen, ground in liquid nitrogen and stored at -80 °C before analysis.
475 For NBT-staining wild type and mutant plants were grown on square Petri dishes (10 x 10 cm). Each
476 Petri dish contained 100 seeds, organized in two contiguous rows (20 seeds) for each genotype.
477 Half-strength Murashige Skoog (MS½) medium containing 1 % (w/v) agar was used. Seeds were
478 sterilized with chlorine smoke for 5 h before being transferred to the Petri dish with the help of a
479 sterilized toothpick. Petri dishes were stored at 4 °C for 4 days in the dark and then transferred to
480 the growth chamber for 14 days with 12/12 h light/dark cycle and photosynthetic photon flux density
481 of 100 µE m^{-2} sec^{-1}.

482

483 *Quantification of ascorbate and anthocyanins*

484 Asc was quantified by adapting the protocol of Queval & Noctor (2007). Briefly, plant powders were
485 suspended in 200 mM HCl by applying a 1:100 ratio between HCl volume and fresh weight. Samples
486 were vortexed and centrifuged at 15,000 rpm for 10 minutes at 4 °C. The resulting cell extracts were
487 neutralized with 200 mM NaOH and 200 mM NaH_2PO_4, pH 5.6. Neutralized samples (120 µl), either
488 reduced with 5 µl of 25 mM DTT for assaying Asc+DHA or used as such for Asc assays, were mixed
489 with 600 µl of NaH_2PO_4 (200 mM, pH 5.6) and 450 µl of MilliQ water. The absorbance at 265 nm
490 was measured spectrophotometrically (Shimadzu UV-1900) before and after the addition of 0.1 units
491 of Asc oxidase from *Cucurbita* sp. (Merck). The assay was performed on three (n=3) or four (n=4)
492 biological replicates for each genotype, with three technical replicates per sample.
493 Anthocyanin content was measured by adapting the method of Giacomelli et al. (2006). The assay
494 was performed on four biological replicates (n=4) for each genotype, with two technical replicates

per sample. Statistical analysis was performed by ANOVA using a 1-way completely randomized model and Tukey's HSD test with 0.05 significance level (CoHort Software, USA).

NBT staining

The superoxide accumulation was qualitatively evaluated in 14 days-old plants grown in agarized MS½. Plants were soaked for 30 min at room temperature in NBT solution (50 mM K-phosphate buffer, pH 7.5; 0.5% (v/v) Triton X-100; 0.01% (w/v) NBT). After staining, plants were bleached in 80% (v/v) ethanol.

Vacuole isolation

Plants of *Arabidopsis thaliana* Columbia-0 wild type and *CYB561A* mutants (see above) were grown on soil in a growth chamber at 22 °C and 8 h light/16 h dark regime. For isolation of mesophyll protoplasts, rosette leaves from 3-10 week-old plants were used. Leaves were cut in strips and incubated for 1 h in enzyme solution containing 0.5% (w/v) Cellulase Onozuka R-10 (Yakult), 0.05% (w/v) Pectolyase Y-23 (Seishin), 0.25% (w/v) Macerozyme R-10, 1 mM $CaCl_2$, 500 mM D-sorbitol, 10 mM MES, pH 5.5. The protoplasts were washed twice, resuspended and maintained in W5 solution (in mM: 125 $CaCl_2$, 154 NaCl, 5 KCl, 2 MES-KOH, 5 glucose, pH 5.6). An efficient vacuole release was obtained just before patch-clamp experiments by perfusion of protoplasts with vacuolar release solution (VRS) containing (in mM): 100 malic acid, 160 Bis-tris-Propane, 5 EGTA, 3 $MgCl_2$, 200 D-sorbitol, pH 7.3.

Patch-clamp recordings

Patch-clamp experiments were performed as described elsewhere (Costa *et al.*, 2012; Boccaccio *et al.*, 2014). Protoplasts were placed in the recording chamber and exposed to vacuolar release solution. Patch-clamp experiments were performed on isolated vacuoles in the whole-vacuole configuration. Standard pipette (vacuolar) solution contained (in mM): 100 KCl, 2 $MgCl_2$, 1 $CaCl_2$, 10 MES, 240 D-sorbitol, pH 5.5 (with KOH); 10 HEPES instead of MES was used in experiments performed at pH 7.5. Standard bath (cytosolic) solution contained (in mM): 100 KCl, 2 $MgCl_2$, 10

HEPES, 290 D-sorbitol, pH 7.5 (with KOH). Potassium hexacyano-ferrate (III) (ferricyanide, FeCN, throughout the paper) was prepared as 100 mM stock and diluted appropriately in luminal or cytosolic standard solutions. L-Ascorbic acid was dissolved at a concentration of 40 mM in luminal or cytosolic standard solutions and pH was adjusted to 7.5 with BTP. The final solution was aliquoted and stored at -20 °C. Asc aliquots were diluted further in standard solution at the desired concentration just before use and kept on ice. Asc oxidase from *Cucurbita* sp. was dissolved in water at a stock concentration of 100 units/ml, aliquoted and stored at -20 °C. Aliquots were diluted in standard solution at a concentration of 2 units/ml just before use. All chemicals were purchased from Merck (Italy, Germany).

Patch pipettes were pulled from borosilicate glass capillaries (Harvard Apparatus, Holliston, MA, USA) and had resistances of 3-5 MΩ. Currents were recorded with a List EPC-7 amplifier (Darmstadt, Germany), filtered with a low pass filter and controlled by the acquisition program Pulse (Heka Elektronik, Lambrecht, Germany). Bath solution changes were performed by a gravity perfusion system for inflow and a peristaltic pump for outflow (Gilson Inc., Middleton, WI, USA); the perfusion system was optimized to change the bath solution in approx. 1 min (Festa *et al.*, 2016). All experiments were performed in continuous perfusion to minimise mechanical interferences. Kinetics of the current traces upon addition or removal of donor/acceptor reflects the speed of perfusion and has no physiological meaning. Membrane capacitance (C_V) could be estimated by the current transient elicited by a 10 mV voltage pulse (Sakmann & Neher, 1995; Carpaneto *et al.*, 2010). By convention, positive currents correspond to electrons/anions moving from the vacuolar lumen to the cytosolic side or to cations moving in the opposite direction.

BCECF fluorescence

Experiments designed to estimate pH changes associated with Asc oxidation were performed as described in (Carpaneto *et al.*, 2017; Gradogna *et al.*, 2021). A concentration of 10 μM BCECF was added to the pipette (vacuolar) solution containing (in mM): 100 KCl, 2 $MgCl_2$, 240 D-sorbitol, pH 7 (with KOH), in the presence or absence (control) of 5 mM Asc. After reaching the whole-vacuole configuration, the process of BCECF loading into the vacuole usually took about 20 min. To increase

the success of the experiment, we started the application of cytosolic FeCN when the pH trace approached its steady-state value. Inside the vacuole, we chose a circular region of interest (ROI), which was excited alternatively at 490 and 440 nm in 100 ms excitation cycles. Excitation light, selected by a monochromator (Cairn Research, Faversham, UK) was generated by a 75-Watt Xenon arc lamp (Osram, Italy). Fluorescence emission was detected using a 515-nm bandpass emission filter by a CCD camera (Roper Scientific, Germany) mounted on an inverted microscope (Axiovert, Zeiss, Germany) and recorded every 300 ms. The fluorescence ratio (490/440) was calculated online (background fluorescence was negligible). Conversion of fluorescence ratios to pH units was performed as in (Carpaneto *et al.*, 2017; Gradogna *et al.*, 2021).

Protoplast transformation

The *CYB561A* coding sequence was PCR amplified from the U15108 clone, purchased from the Arabidopsis Biological Resources Stock Centre (Columbus, Ohio, USA). The primers used for the PCR reaction (U15108LXHOI: 5'-ACTCGAGATGGCTGTCCGGATAAAC-3'; U15108RECORI: 5'-GAATTCTATAGCAGAATAACTGAAGTCAAC-3') carried the restriction sites for XhoI and EcoRI, respectively, and allowed the insertion of the coding sequence into the pSAT vector, in frame with the sequence of a downstream EGFP. The pSAT-CYB561A:EGFP construct was finally validated by Sanger sequencing.

Mesophyll protoplasts were isolated from well expanded leaves from four weeks old plants and transiently transformed using the polyethylene glycol method as described elsewhere (Yoo *et al.*, 2007; Festa *et al.*, 2022; Gradogna & Carpaneto, 2022). Confocal microscopy analysis of vacuoles expressing the CYB561A-EGFP protein was performed using a Leica SP2 (http://www.leica-microsystems.com) laser-scanning confocal imaging system. For EGFP and FM4-64 fluorescence, excitation was set at 488 nm and detection ranges were 515 to 530 nm and 575 to 625 nm, respectively.

Data analysis

The effects of Asc or FeCN were estimated by subtracting the current in control condition from the steady-state current elicited by the presence of the reductant or oxidant. Currents were divided by the tonoplast capacitance (current densities) to compare data obtained from vacuoles of different sizes.

Unless otherwise indicated, data are shown as mean ± standard error, with *n* indicating the number of independent experiments. Data analysis, figures and models were done with Igor software (Wavemetrics, Lake Oswego, OR, USA).

Mathematical model

The following extended Michaelis-Menten equation was used to fit experimental currents upon variation of both cytosolic/vacuolar Asc and FeCN at a fixed tonoplast voltage of 0 mV:

$I=I_{max}/ (K_A/[A] + K_F/[F] + 1)$ equation 1

I is the experimental current, [A] and [F] are the concentrations of Asc and FeCN respectively. Equation 1, which was developed by a simple kinetic model (Picco *et al.*, 2014), has only three free parameters i.e. the maximum current I_{max}, the two constants K_A and K_F, which can be interpreted as the affinity constants for Asc and FeCN, respectively.

Acknowledgement

We thank Ricardo F. H. Giehl and Nicolaus von Wiren (Leibniz-Institute of Plant Genetics and Crop Plant Research, Germany) for critical reading and suggestions, Ekkehard Neuhaus and Ruth Wartenberg (University of Kaiserslautern, Germany) for collaboration and assistance in localization studies, Natasha Balasubramaniam (University of Genoa) for support in transformation experiments and Francesca Quartino (IBF-CNR, Italy) for technical assistance.

Author contributions

PT and AC designed the research, AG, LL, SB, ET, JSS, FS performed the research, AG, ET, JSS,

606 CP, FS, PT and AC analysed the data, AG and PT wrote the manuscript, LL, ET, JSS, CP, FS and
607 AC revised the manuscript.
608

REFERENCES

Anschau V, Ferrer-Sueta G, Aleixo-Silva RL, Bannitz Fernandes R, Tairum CA, Tonoli CCC, Murakami MT, de Oliveira MA, Netto LES. **2020**. Reduction of sulfenic acids by ascorbate in proteins, connecting thiol-dependent to alternative redox pathways. *Free Radical Biology & Medicine* **156**: 207–216.

Asard H, Barbaro R, Trost P, Bérczi A. **2013**. Cytochromes b561: ascorbate-mediated trans-membrane electron transport. *Antioxidants & Redox Signaling* **19**: 1026–1035.

Bérczi A, Zimányi L. **2014**. The trans-membrane cytochrome b561 proteins: structural information and biological function. *Current Protein & Peptide Science* **15**: 745–760.

Bethmann B, Thaler M, Simonis W, Schonknecht G. **1995**. Electrochemical Potential Gradients of H+, K+, Ca2+, and Cl- across the Tonoplast of the Green Alga Eremosphaera Viridis. *Plant Physiology* **109**: 1317–1326.

Boccaccio A, Scholz-Starke J, Hamamoto S, Larisch N, Festa M, Gutla PVK, Costa A, Dietrich P, Uozumi N, Carpaneto A. **2014**. The phosphoinositide PI (3, 5) P2 mediates activation of mammalian but not plant TPC proteins: functional expression of endolysosomal channels in yeast and plant cells. *Cellular and Molecular Life Sciences* **71**: 4275–4283.

Carpaneto A, Boccaccio A, Lagostena L, Di Zanni E, Scholz-Starke J. **2017**. The signaling lipid phosphatidylinositol-3,5-bisphosphate targets plant CLC-a anion/H+ exchange activity. *EMBO reports* **18**: 1100–1107.

Carpaneto A, Koepsell H, Bamberg E, Hedrich R, Geiger D. **2010**. Sucrose-and H+-dependent charge movements associated with the gating of sucrose transporter ZmSUT1. *PLoS One* **5**: e12605.

Costa A, Gutla PVK, Boccaccio A, Scholz-Starke J, Festa M, Basso B, Zanardi I, Pusch M, Schiavo FL, Gambale F, *et al.* 2012. The Arabidopsis central vacuole as an expression system for intracellular transporters: functional characterization of the Cl-/H+ exchanger CLC-7. *The Journal of Physiology* **590**: 3421–3430.

Csepregi K, Hideg É. **2018**. Phenolic Compound Diversity Explored in the Context of Photo-Oxidative Stress Protection. *Phytochemical analysis: PCA* **29**: 129–136.

Ferreres F, Figueiredo R, Bettencourt S, Carqueijeiro I, Oliveira J, Gil-Izquierdo A, Pereira DM, Valentão P, Andrade PB, Duarte P, *et al.* 2011. Identification of phenolic compounds in isolated vacuoles of the medicinal plant Catharanthus roseus and their interaction with vacuolar class III peroxidase: an H_2O_2 affair? *Journal of Experimental Botany* **62**: 2841–2854.

Festa M, Lagostena L, Carpaneto A. **2016**. Using the plant vacuole as a biological system to investigate the functional properties of exogenous channels and transporters. *Biochimica Et Biophysica Acta* **1858**: 607–612.

Festa M, Minicozzi V, Boccaccio A, Lagostena L, Gradogna A, Qi T, Costa A, Larisch N, Hamamoto S, Pedrazzini E, *et al.* 2022. Current Methods to Unravel the Functional Properties of Lysosomal Ion Channels and Transporters. *Cells* **11**: 921.

Foyer CH, Kyndt T, Hancock RD. **2020**. Vitamin C in Plants: Novel Concepts, New Perspectives, and Outstanding Issues. *Antioxidants & Redox Signaling* **32**: 463–485.

Ganasen M, Togashi H, Takeda H, Asakura H, Tosha T, Yamashita K, Hirata K, Nariai Y, Urano T, Yuan X, *et al.* 2018. Structural basis for promotion of duodenal iron absorption by enteric ferric reductase with ascorbate. *Communications Biology* **1**: 120.

Giacomelli L, Rudella A, van Wijk KJ. **2006**. High light response of the thylakoid proteome in arabidopsis wild type and the ascorbate-deficient mutant vtc2-2. A comparative proteomics study. *Plant Physiology* **141**: 685–701.

Gradogna A, Carpaneto A. **2022**. Electrophysiology and fluorescence to investigate cation channels and transporters in isolated plant vacuoles. *Stress Biology* **2**: 42.

Gradogna A, Scholz-Starke J, Pardo JM, Carpaneto A. **2021**. Beyond the patch-clamp resolution: functional activity of nonelectrogenic vacuolar NHX proton/potassium antiporters and inhibition by phosphoinositides. *The New Phytologist* **229**: 3026–3036.

Griesen D, Su D, Bérczi A, Asard H. **2004**. Localization of an ascorbate-reducible cytochrome b561 in the plant tonoplast. *Plant Physiology* **134**: 726–734.

Hedrich R. **2012**. Ion channels in plants. *Physiological Reviews* **92**: 1777–1811.

Heyneke E, Luschin-Ebengreuth N, Krajcer I, Wolkinger V, Müller M, Zechmann B. **2013**. Dynamic compartment specific changes in glutathione and ascorbate levels in Arabidopsis plants exposed to different light intensities. *BMC plant biology* **13**: 104.

Hoang MTT, Almeida D, Chay S, Alcon C, Corratge-Faillie C, Curie C, Mari S. **2021**. AtDTX25, a member of the multidrug and toxic compound extrusion family, is a vacuolar ascorbate transporter that controls intracellular iron cycling in Arabidopsis. *The New Phytologist* **231**: 1956–1967.

Hossain MA, Asada K. **1985**. Monodehydroascorbate reductase from cucumber is a flavin adenine dinucleotide enzyme. *The Journal of Biological Chemistry* **260**: 12920–12926.

Klein M, Deniz E, Heit S, Wille G, Mäntele W, Lancaster CRD. **2020**. Proton-Coupled Electron Transport in Two Distinct CYBASC Paralogs of Arabidopsis thaliana: A Comparative Characterization of Highly Conserved Tyrosine and Lysine Residues. *Biochemistry* **59**: 2328–2339.

Lu P, Ma D, Yan C, Gong X, Du M, Shi Y. **2014**. Structure and mechanism of a eukaryotic transmembrane ascorbate-dependent oxidoreductase. *Proceedings of the National Academy of Sciences of the United States of America* **111**: 1813–1818.

Lüthje S, Martinez-Cortes T. **2018**. Membrane-Bound Class III Peroxidases: Unexpected Enzymes with Exciting Functions. *International Journal of Molecular Sciences* **19**: E2876.

Miyaji T, Kuromori T, Takeuchi Y, Yamaji N, Yokosho K, Shimazawa A, Sugimoto E, Omote H, Ma JF, Shinozaki K, *et al.* 2015. AtPHT4;4 is a chloroplast-localized ascorbate transporter in Arabidopsis. *Nature Communications* **6**: 5928.

Moran N, Ehrenstein G, Iwasa K, Bare C, Mischke C. **1984**. Ion channels in plasmalemma of wheat protoplasts. *Science (New York, N.Y.)* **226**: 835–838.

Munné-Bosch S, Müller M. **2013**. Hormonal cross-talk in plant development and stress responses. *Frontiers in Plant Science* **4**: 529.

Nakanishi N, Rahman MM, Sakamoto Y, Miura M, Takeuchi F, Park S-Y, Tsubaki M. **2009**. Inhibition of electron acceptance from ascorbate by the specific N-carbethoxylations of maize cytochrome b561: a common mechanism for the transmembrane electron transfer in cytochrome b561 protein family. *Journal of Biochemistry* **146**: 857–866.

Nanasato Y, Akashi K, Yokota A. **2005**. Co-expression of cytochrome b561 and ascorbate oxidase in leaves of wild watermelon under drought and high light conditions. *Plant & Cell Physiology* **46**: 1515–1524.

Njus D, Kelley PM, Tu Y-J, Schlegel HB. **2020**. Ascorbic acid: The chemistry underlying its antioxidant properties. *Free Radical Biology & Medicine* **159**: 37–43.

Noctor G. **2006**. Metabolic signalling in defence and stress: the central roles of soluble redox couples. *Plant, Cell & Environment* **29**: 409–425.

Noctor G, Foyer CH. **2016**. Intracellular Redox Compartmentation and ROS-Related Communication in Regulation and Signaling. *Plant Physiology* **171**: 1581–1592.

Noctor G, Reichheld J-P, Foyer CH. **2018**. ROS-related redox regulation and signaling in plants. *Seminars in Cell & Developmental Biology* **80**: 3–12.

Page M, Sultana N, Paszkiewicz K, Florance H, Smirnoff N. **2012**. The influence of ascorbate on anthocyanin accumulation during high light acclimation in Arabidopsis thaliana: further evidence for redox control of anthocyanin synthesis. *Plant, Cell & Environment* **35**: 388–404.

Park AK, Kim I-S, Do H, Jeon BW, Lee CW, Roh SJ, Shin SC, Park H, Kim Y-S, Kim Y-H, *et al.* 2016. Structure and catalytic mechanism of monodehydroascorbate reductase, MDHAR, from Oryza sativa L. japonica. *Scientific Reports* **6**: 33903.

Picco C, Scholz-Starke J, Festa M, Costa A, Sparla F, Trost P, Carpaneto A. **2015**. Direct Recording of Trans-Plasma Membrane Electron Currents Mediated by a Member of the Cytochrome b561 Family of Soybean. *Plant Physiology* **169**: 986–995.

Picco C, Scholz-Starke J, Naso A, Preger V, Sparla F, Trost P, Carpaneto A. **2014**. How are cytochrome b561 electron currents controlled by membrane voltage and substrate availability? *Antioxidants & Redox Signaling* **21**: 384–391.

Plumb W, Townsend AJ, Rasool B, Alomrani S, Razak N, Karpinska B, Ruban AV, Foyer CH. **2018**. Ascorbate-mediated regulation of growth, photoprotection, and photoinhibition in Arabidopsis thaliana. *Journal of Experimental Botany* **69**: 2823–2835.

Potters G, Horemans N, Bellone S, Caubergs RJ, Trost P, Guisez Y, Asard H. **2004**.

Dehydroascorbate influences the plant cell cycle through a glutathione-independent reduction mechanism. *Plant Physiology* **134**: 1479–1487.

Preger V, Scagliarini S, Pupillo P, Trost P. **2005**. Identification of an ascorbate-dependent cytochrome b of the tonoplast membrane sharing biochemical features with members of the cytochrome b561 family. *Planta* **220**: 365–375.

Queval G, Noctor G. **2007**. A plate reader method for the measurement of NAD, NADP, glutathione, and ascorbate in tissue extracts: Application to redox profiling during Arabidopsis rosette development. *Analytical Biochemistry* **363**: 58–69.

Rautenkranz A a. F, Li L, Machler F, Martinoia E, Oertli JJ. **1994**. Transport of Ascorbic and Dehydroascorbic Acids across Protoplast and Vacuole Membranes Isolated from Barley (Hordeum vulgare L. cv Gerbel) Leaves. *Plant Physiology* **106**: 187–193.

Sakmann B, Neher E. **1995**. *Single-channel recording*. Plenum Press - New York and London.

Schroeder JI, Hedrich R, Fernandez JM. **1984**. Potassium-selective single channels in guard cell protoplasts of Vicia faba. *Nature* **312**: 361–362.

Shitan N, Yazaki K. **2020**. Dynamism of vacuoles toward survival strategy in plants. *Biochimica Et Biophysica Acta. Biomembranes* **1862**: 183127.

Smirnoff N. **2018**. Ascorbic acid metabolism and functions: A comparison of plants and mammals. *Free Radical Biology & Medicine* **122**: 116–129.

Smirnoff N, Arnaud D. **2019**. Hydrogen peroxide metabolism and functions in plants. *The New Phytologist* **221**: 1197–1214.

Smith EN, Schwarzländer M, Ratcliffe RG, Kruger NJ. **2021**. Shining a light on NAD- and NADP-based metabolism in plants. *Trends in Plant Science* **26**: 1072–1086.

Takahama U. **2004**. Oxidation of vacuolar and apoplastic phenolic substrates by peroxidase: Physiological significance of the oxidation reactions. *Phytochemistry Reviews* **3**: 207–219.

Terai Y, Ueno H, Ogawa T, Sawa Y, Miyagi A, Kawai-Yamada M, Ishikawa T, Maruta T. **2020**. Dehydroascorbate Reductases and Glutathione Set a Threshold for High-Light-Induced Ascorbate Accumulation. *Plant Physiology* **183**: 112–122.

Tsubaki M, Takeuchi F, Nakanishi N. **2005**. Cytochrome b561 protein family: expanding roles and versatile transmembrane electron transfer abilities as predicted by a new classification system and protein sequence motif analyses. *Biochimica Et Biophysica Acta* **1753**: 174–190.

Walker DJ, Leigh RA, Miller AJ. **1996**. Potassium homeostasis in vacuolate plant cells. *Proceedings of the National Academy of Sciences of the United States of America* **93**: 10510–10514.

Wimalasena K, Dharmasena S. **1994**. Substrate specificity of ascorbate oxidase: unexpected similarity to the reduction site of dopamine beta-monooxygenase. *Biochemical and Biophysical Research Communications* **203**: 1471–1476.

Yoo S-D, Cho Y-H, Sheen J. **2007**. Arabidopsis mesophyll protoplasts: a versatile cell system for transient gene expression analysis. *Nature Protocols* **2**: 1565–1572.

Zaffagnini M, Fermani S, Marchand CH, Costa A, Sparla F, Rouhier N, Geigenberger P, Lemaire SD, Trost P. **2019**. Redox Homeostasis in Photosynthetic Organisms: Novel and Established Thiol-Based Molecular Mechanisms. *Antioxidants & Redox Signaling* **31**: 155–210.

Zechmann B. **2018**. Compartment-Specific Importance of Ascorbate During Environmental Stress in Plants. *Antioxidants & Redox Signaling* **29**: 1488–1501.

Zheng X-T, Yu Z-C, Tang J-W, Cai M-L, Chen Y-L, Yang C-W, Chow WS, Peng C-L. **2021**. The major photoprotective role of anthocyanins in leaves of Arabidopsis thaliana under long-term high light treatment: antioxidant or light attenuator? *Photosynthesis Research* **149**: 25–40.

Zipor G, Duarte P, Carqueijeiro I, Shahar L, Ovadia R, Teper-Bamnolker P, Eshel D, Levin Y, Doron-Faigenboim A, Sottomayor M, *et al.* 2015. In planta anthocyanin degradation by a vacuolar class III peroxidase in Brunfelsia calycina flowers. *The New Phytologist* **205**: 653–665.

771 Tables

772

773 **Table 1** – Steady state kinetic parameters of the Asc-dependent trans-tonoplast electron transport
774 in isolated vacuoles from Arabidopsis mesophyll protoplasts in the presence of ferricyanide as
775 electron acceptor

776

recording mode	Electron donor Ascorbate K_A (mM)	Electron acceptor Ferricyanide K_F (mM)	Maximal electron transport rate I_{max} (pA/pF)
cytosolic Asc/vacuolar FeCN	K_{Ac}=51±8	K_{Fv}=1.0±0.2	I_{cvmax}=3.7±0.5
vacuolar Asc/cytosolic FeCN	K_{Av}=4.5±1.0	K_{Fc}=0.024±0.002	I_{vcmax}=3.1±0.5

777

778

779

780 **Figure legends**

781

782 **Figure 1: Cytosolic ascorbate elicits electron currents in the presence of vacuolar FeCN.**
783 (a) Typical membrane currents elicited by the application of 10 mM Asc in the absence (upper trace)
784 and in the presence (lower trace) of 1 mM vacuolar FeCN. (b) Varying cytosolic ions and vacuolar
785 pH doesn't change the response to Asc. Current amplitudes elicited by cytosolic 10 mM Asc in
786 modified bath solutions and vacuolar pH (condition A: control, cytosolic KCl 100 mM / vacuolar pH
787 5.5 (standard pipette solution at pH 5.5), condition B: cytosolic BTP-MES 100 mM replaces KCl /
788 vacuolar pH 5.5, condition C: cytosolic BTP-MES 100 mM / vacuolar pH 6.5), in the absence and
789 presence (+) of 1 mM vacuolar FeCN. Standard bath solution at pH 7.5. Current amplitudes elicited
790 by ascorbate were normalised to membrane capacitance (A: n=6, B: n=6, C: n=3, A+: n=5, B+: n=6,
791 C+: n=5). (c and d) Specificity of ascorbate effect. (c) Current recording from a vacuole loaded with
792 1 mM vacuolar FeCN upon exposure (horizontal bars) to cytosolic DTT and Asc both at 10 mM. The
793 letters above the bars indicate significant differences (one-way ANOVA followed by post hoc Tukey's
794 test, $P < 0.05$). (d) Current amplitudes elicited by 10 mM DTT and 10 mM Asc normalised to
795 membrane capacitance (DTT: n=6; Asc: n=6). Statistical significance (according to Student's t-test):
796 ***$P < 0.001$.

797

798 **Figure 2: Electron currents depend on cytosolic ascorbate and vacuolar FeCN concentrations.**
799 (a) Dependence of electron currents on cytosolic Asc ($[Asc]_{cyt}$) at three different vacuolar FeCN
800 concentrations (FeCN 0.3 mM: Asc from 2.5 to 20 mM n=4, Asc 40 mM n=3; FeCN 1 mM: Asc 2.5
801 mM n=8, Asc from 10 to 40 mM n=9; FeCN 3 mM: Asc 2.5 and 10 mM n=11, Asc 5, 20 and 40 mM
802 n=12); pH was 7.5 and 5.5 in the standard bath and pipette solutions, respectively. At each FeCN
803 concentration, data points were fitted (continuous lines) by the Michaelis–Menten function:
804 $I=I_{Acmax}^{app}/(K_{Ac}^{app}/[Asc]_{cyt} + 1)$. (b and c) The apparent maximum current at saturating cytosolic Asc,
805 I_{Acmax}^{app} (b), and the apparent affinity constant for Asc, K_{Ac}^{app} (c), both derived from the data fit in (a),
806 are plotted as a function of external FeCN. (d) Dependence of electron currents on vacuolar FeCN
807 ($[FeCN]_{vac}$) at different cytosolic Asc. At each Asc concentration, data points were fitted the

Michaelis–Menten function $I=I_{Fvmax}^{app}/(K_{Fv}^{app}/[FeCN]_{vac} + 1)$, continuous lines. (e and f) The apparent maximum current at saturating FeCN, I_{Fvmax}^{app} (f), and the apparent affinity constant for FeCN, K_{Fv}^{app} (g), both derived from the data fit in (e), are plotted as a function of the cytosolic Asc. Continuous lines in (b and c) and (e and f) were obtained by a global fit of the data using Equation 1, see Methods and Table 1.

Figure 3: Vacuolar ascorbate elicits electron currents in the presence of cytosolic FeCN. (a) Examples of current recordings upon the addition of 100 µM cytosolic FeCN in different pipette (vacuolar) solutions (top: control, middle: control with 5 mM Asc, bottom: control with 5 mM DTT); standard bath and pipette solutions with symmetrical pH of 7.5. (b) Histogram of the current amplitudes evoked by 100 µM cytosolic FeCN in the same vacuolar conditions shown in (a). Current amplitudes were normalised to membrane capacitance (control: n=6, Asc: n=7, DTT: n=4). Statistical significance (according to Student's t-test): ***P < 0.001.

Figure 4 Electron currents depend on vacuolar ascorbate and cytosolic FeCN concentrations. (a) Current trace recorded in the presence of 5 mM vacuolar Asc in response to increasing cytosolic FeCN (in micromolar). (b) Dependence of electron currents on cytosolic FeCN at different vacuolar Asc concentrations (1 mM: n=3 (FeCN 3.3 and 100 µM) and n=4 (FeCN 10 and 33 µM); 5 mM: n=5 (FeCN 3.3), n=6 (FeCN 10 and 33 µM) and n=7 (FeCN 100 µM); 20 mM: n=4; 40 mM: n=4 (FeCN 3.3 and 10 µM) and n=6 (FeCN 33 and 100 µM)); pH in the standard bath and pipette solutions was symmetric and equal to 7.5. At each FeCN concentration, data points were fitted (continuous lines) by the Michaelis–Menten function: $I=I_{Fcmax}^{app}/(K_{Fc}^{app}/[FeCN]_{cyt} + 1)$. (c and d) The apparent maximum current at saturating cytosolic FeCN, I_{Fcmax}^{app} (c), and the apparent affinity constant for FeCN, K_{Fc}^{app} (d), both derived from the data fit in (b), are displayed as a function of cytosolic FeCN. (e) Dependence of electron currents on vacuolar Asc at different cytosolic FeCN. At each FeCN concentration, data points were fitted (continuous lines) by the Michaelis–Menten function $I=I_{Avmax}^{app}/(K_{Av}^{app}/[Asc]_{vac} + 1)$. (f and g) The apparent maximum current at saturating Asc, I_{Avmax}^{app} (f), and the apparent affinity constant for vacuolar Asc, K_{Av}^{app} (g), both derived from the data fit in (E),

are plotted as a function of cytosolic FeCN. Continuous lines in (c and d) and (e and f) were obtained by a global fit of the data using Equation 1, see Methods and Table 1.

Figure 5: Vacuolar acidification is associated with electron transport elicited by vacuolar ascorbate and cytosolic FeCN.

(a) Increase of cytosolic FeCN induced a significant drop of vacuolar pH, which was recorded by the proton-sensitive probe BCECF added at 10 μM in the standard pipette (vacuolar) solution (upper panel, see Methods). Vacuolar Asc was 5 mM; standard bath solution at pH 7.5. The lower panel shows synchronised patch-clamp recordings at a holding potential of 0 mV. Currents increased upon addition of cytosolic FeCN. (b) Histogram of pH changes elicited by FeCN in the presence and absence of vacuolar Asc (Asc 5 mM: n=3 (FeCN 3.3 μM), n=4 (FeCN 10 μM), n=6 (FeCN 100 μM); without vacuolar Asc: n=4 (FeCN 100 μM). Statistical significance (according to Student's t-test): ***P < 0.001.

Figure 6: CYB561A mutant plants lack the electron currents elicited by ascorbate and FeCN.

(a) Both *cyb561a-1* and *cyb561a-2* mutant lines, upon application of 10 mM cytosolic Asc (horizontal bar), in the presence of 1 mM vacuolar FeCN, did not show any current change. (b) Current amplitudes, normalized to membrane capacitance, elicited by 10 mM cytosolic Asc in vacuoles from wild-type (WT: n=9) and mutant plants (*cyb561a-1*: n=9, *cyb561a-2*: n=8); pH was 7.5 and 5.5 in standard bath and pipette solutions, respectively.

(c) In the opposite experimental configuration, addition of 100 μM cytosolic FeCN (horizontal bar), with vacuolar Asc from 5 to 40 mM, did not induce electron currents in mutant lines. (d) Mean current amplitudes in vacuoles from wild-type (WT: n=24) and mutant plants (*cyb561a-1*: n=18, *cyb561a-2*: n=9); standard bath and pipette solutions with symmetrical pH equal to 7.5. Statistical significance (according to Student's t-test): ***P < 0.001.

Figure 7: MDHA is an electron acceptor of vacuolar CYB561A.

a) Scheme of the experiment: Asc and AO solutions indicate the cytosolic solutions containing Ascorbate and Ascorbate Oxidase, respectively. At the interface of the two solutions, the interaction between Asc and AO generated MDHA, which subsequently dismutates to Asc and dehydroascorbate (DHA). MDHA, whose concentration is predicted to depend on both the reaction rate of AO and the dismutation rate of MDHA, could reach the vacuole with the perfusion flow. (b) Currents elicited by application of cytosolic MDHA (horizontal bars) in vacuoles from wild type (WT) and mutant (*cyb561a-1* and *cyb561a-2*) Arabidopsis plants. Holding voltage of 0 mV. Gaps in the current traces correspond to the application of 200 ms voltage ramps from -80 to +80 mV (not shown for the sake of clarity; see Suppl. Fig. 6). The vacuole was consecutively perfused with a bath solution containing Ascorbate oxidase at a concentration of 2 u/ml and then changed with a solution containing 0.5 mM Asc. MDHA was generated at the interface of the two solutions. (c) Current amplitudes, normalized to membrane capacitance, elicited by MDHA in vacuoles from wild-type (WT: n=7) and mutant plants (*cyb561a-1*: n=4, *cyb561a-2***:** n=5). (d) Electron currents versus Asc used to generate MDHA in the cytosolic bath solution. Vacuoles were consecutively perfused with a bath solution containing 2 u/ml of Ascorbate oxidase (AO-solution) and then changed with bath solution containing different concentrations (Asc 0.03 mM n=3, Asc from 0.1 to 5 mM n=7 and Asc 20 mM; n=4) of Asc (Asc-solution); standard bath and pipette solutions with symmetrical pH equal to 7.5.

Fig. 8. Phenotyping of wild-type and *cyb561a* mutant plants.

(a and b) Plants (n=45) were grown for 14 days on agarized MS1/2 medium plates in control conditions (100 µE m^{-2} s^{-1}). Asc (colored bars) and DHA (white bars) were measured spectrophotometrically (a), and ROS were qualitatively assessed with the NBT staining (b). (c and e) Plants were grown for 48 days on soil in control conditions and then exposed to HL (700 µE m^{-2} s^{-1}) for 4, 7 and 11 days. Asc (colored bars), DHA (white bars) (c) and anthocyanins (d) were determined spectrophotometrically. (a, c, d) Values are reported as means ± SE obtained from n=3 (panel a) or n=4 (panel c) independent biological replicates. Statistical analyses performed with 1-way completely randomized ANOVA, using the Tukey's HSD test with significance level of 0.05. In

890 panels a and c, ANOVA was run on Asc and Asc+DHA data independently. Letters in the bars refer
891 to Asc data, letters above the bars refer to Asc+DHA data.
892

Supplemental Figure legends

Supplemental Figure 1 Voltage dependence of electron currents elicited by cytosolic ascorbate and vacuolar FeCN.

(a) Membrane currents elicited by a series of voltage steps ranging from -60 to +60 mV in 20 mV steps were recorded in control condition (con, red traces), in the presence of 10 mM cytosolic Asc (+Asc, blue traces) and after Asc washout (rec, green traces). The pH of cytosolic solution was 7.5. The pipette solution, which is present inside the vacuole, was without FeCN at pH 5.5 in the top panel, with FeCN 1 mM at pH 5.5 in the middle panel and with FeCN 1 mM at pH 7.5 in the bottom panel. (b) I-V relationships of steady-state currents of data shown in a. (c) Current density versus voltage elicited by 10 mM cytosolic Asc (cytosolic pH was 7.5) in different vacuolar solutions: at pH 5.5 (light red bars, n=4), after addition of 1 mM FeCN at pH 5.5 (dark blue bars, n=7) and after addition of 1 mM FeCN at pH 7.5 (grey bars, n=4). Current density at a fixed voltage was obtained by subtracting to the current elicited at 10 mM cytosolic Asc the control current recorded without Asc and normalising by the vacuole capacitance. Significance (according to Student's t-test): * $P<0.05$; ** $P<0.01$; *** $P < 0.001$. In the presence of 1 mM vacuolar FeCN and 10 mM cytosolic Asc, at luminal pH 5.5 and 7.5 there was no significant difference in current densities, indicating that the activity of a possible ascorbate/proton antiporter was negligible in our experimental conditions.

Supplemental Figure 2 Voltage dependence of electron currents elicited by cytosolic FeCN and vacuolar ascorbate.

(a) Membrane currents elicited by a series of voltage steps ranging from -60 to 60 mV in 20 mV steps were recorded in control condition (control, red traces), in the presence of 33 µM FeCN (+FeCN, violet traces) and after FeCN washout (recovery, green traces). Currents were recorded in the absence, top panel, and presence of 5 mM vacuolar Asc. The pH of both cytosolic and vacuolar solutions was 7.5. (b) I-V relationships of steady-state currents of data shown in a. (c) Current density versus voltage elicited by 33 µM cytosolic FeCN in vacuolar solutions without (light red bars, n=3), or with 5 mM Asc (dark violet bars, n=3). Current density at a fixed voltage was obtained by

subtracting the control current recorded in the absence of cytosolic FeCN from the current elicited by 33 μM FeCN. The difference was divided by the vacuole capacitance. Statistical significance (according to Student's t-test): ***P < 0.001.

Supplemental Figure 3 Localization of CYB561-A by confocal microscopy.

Confocal images of a representative vacuole isolated by lysis of a CYB561A:EGFP-expressing protoplast. (a) Bright field. (b) Green fluorescence of CYB561A:EGFP at the vacuolar membrane. (c) Staining of the tonoplast with the membrane marker FM4–64 applied at a final concentration of 5 μM. (d) Overlay. Scale bar: 20 μm.

Supplemental Figure 4 Genetic characterization of cyb561a-1 and cyb561a-2 T-DNA lines.

(a) Map of the two T-DNA insertions (*cyb561a-1* and *cyb561a-2*) in *CYB561A* (*At4g25570*) gene. Black boxes represent exons, black lines represent introns and triangles indicate the insertion site of the T-DNA in each mutant line.

(b) PCR analyses performed to select homozygous T-DNA lines. Genomic DNA amplifications were carried out with the following pairs of primers: lane 1, cyb561a-1 fw + cyb561a-1 rev; lane 2, cyb561a-1 fw + LBb1.3; lane 3, cyb561a-2 fw + cyb561a-2 rev; lane 4, cyb561a-2 fw + LBb1.3.

(c) RT-PCR detection of the residual expression of *CYB561A* in both T-DNA insertion mutants and wild-type plants. Expression levels of *CYB561A* were normalized over the expression levels of ACT8. Quantification was performed with ImageJ. Values are reported as means ± SD obtained from three independent replicates for each genotype. Statistical analyses were performed using Student's t-test. * p ≤ 0.05.

Supplemental Figure 5 Vacuolar ascorbate and cytosolic FeCN did not induce vacuolar acidification in *cyb561a-2* mutant plant.

(a) The presence of 100 μM FeCN in the cytosolic solution did not induce a significant luminal pH change in vacuoles isolated from *cyb561a-2* mutant plants (top panel). The pH was detected by 10 μM BCECF added in the pipette (vacuolar) solution (see Methods). Vacuolar Asc was 5 mM.

Synchronised patch-clamp recordings were shown in the bottom panel (holding potential of 0 mV). Currents were not modified upon addition of cytosolic FeCN. (b) Histogram of pH changes elicited by FeCN in the presence of 5 mM vacuolar Asc, in wild-type (WT: n=7) and *cyb561a-2* (*cyb561a-2*: n=3) plants. Statistical significance (according to Student's t-test): ***P < 0.001.

Supplemental Figure 6 Voltage dependence of electron currents elicited by cytosolic MDHA and vacuolar Asc.

(a) Currents elicited by voltage ramps of 200 ms from -80 to +80 mV in the presence (pink traces) and absence (black traces) of MDHA. Currents were recorded in vacuoles from wild-type (WT, left panel) and mutant (*cyb561a-1*, middle panel and *cyb561a-2*, right panel) plants. The green trace in the left panel was the recovery current recorded at the end of the experiment in the absence of MDHA. Smooth pink and black traces in the left panel were obtained by fitting the experimental currents with polynomial functions and were used to calculate the value of the current at a definite voltage. Cytosolic MDHA was generated as described in the legend of Fig. 7a; the concentration of Asc in the pipette (luminal side) was 5 mM; symmetrical pH equal to 7.5. (b) I-V relationships of currents activated by MDHA after subtraction of currents recorded in the absence of MDHA in wild-type (WT: n=7, pink bars) and mutant (*cyb561a-1*: n=4, and *cyb561a-1*: n=5, respectively red and black bars) plant. Significance (according to Student's t-test): * P<0.05; ** P<0.01; ***P < 0.001. These experiments showed that currents mediated by CYB561A due to the movement of electrons from vacuolar Asc to cytosolic MDHA were active at physiological tonoplast voltages and increased upon voltage increase.

Supplemental Figure 7 - Asc redox state in whole leaf extracts of different genotypes and different growth conditions

(a) The Asc redox state, expressed as Asc/(Asc+DHA) ratio, was determined in 14 days old plants grown on agarized MS1/2 medium plates in control conditions (100 µE m^{-2} s^{-1}, 12/12 h light/dark cycle). Same experiment of Fig. 8a. Statistical analyses performed with 1-way completely

randomized ANOVA, using the Tukey's HSD test with significance level of 0.05 identified no significant differences among genotypes.

(b) The Asc redox state, expressed as Asc/(Asc+DHA) ratio, was determined in plants grown for 48 days on soil in control conditions and then exposed to HL (700 µE m^{-2} s^{-1}) for 4, 7 and 11 days. Same experiment of Fig. 8c. Statistical analyses performed with 1-way completely randomized ANOVA, using the Tukey's HSD test with significance level of 0.05 identified no significant differences among average values for any genotype and time point.

Supplemental Figure 8 – Anthocyanin accumulation in high light

Plants grown for 48 days on soil in control conditions and then exposed to HL (700 µE m^{-2} s^{-1}) for 11 days. Same experiment of Fig. 8d. Picture taken after 4 days of HL treatment already show a stronger pigmentation in *cyb561a* mutant lines in respect to wild type plants.

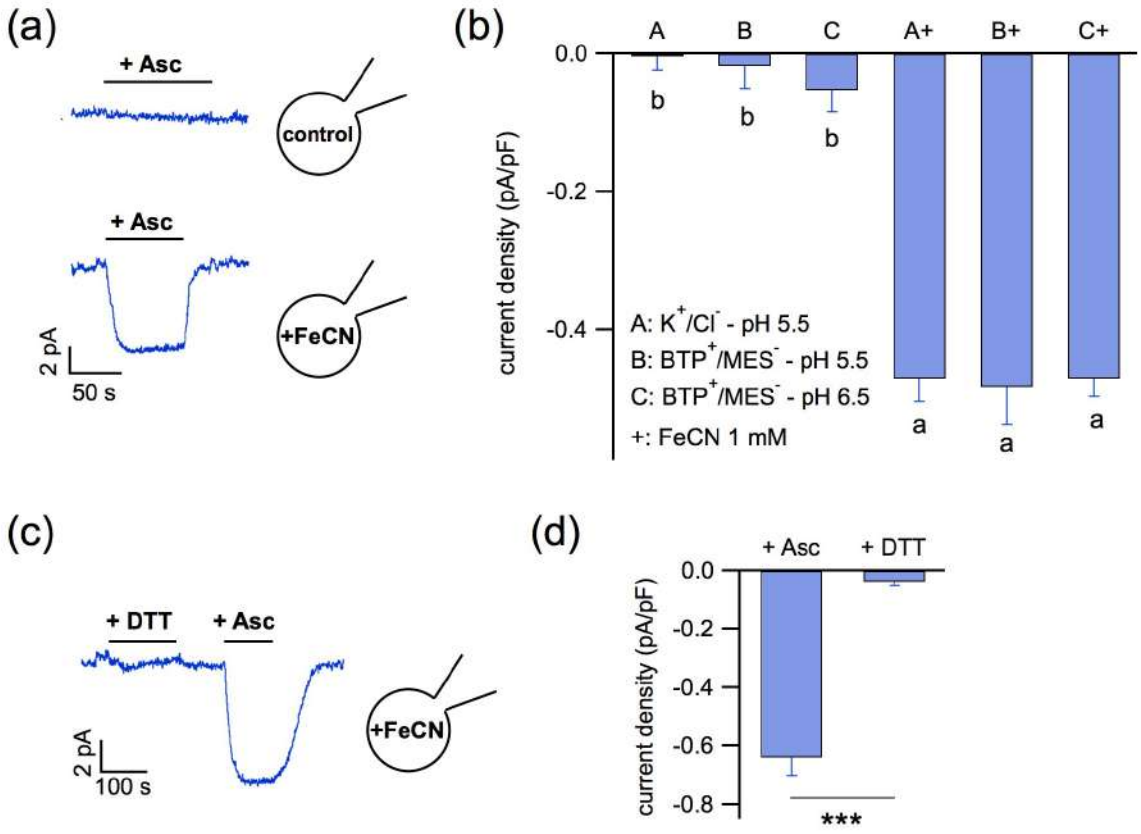

989

990 **Figure 1**

991

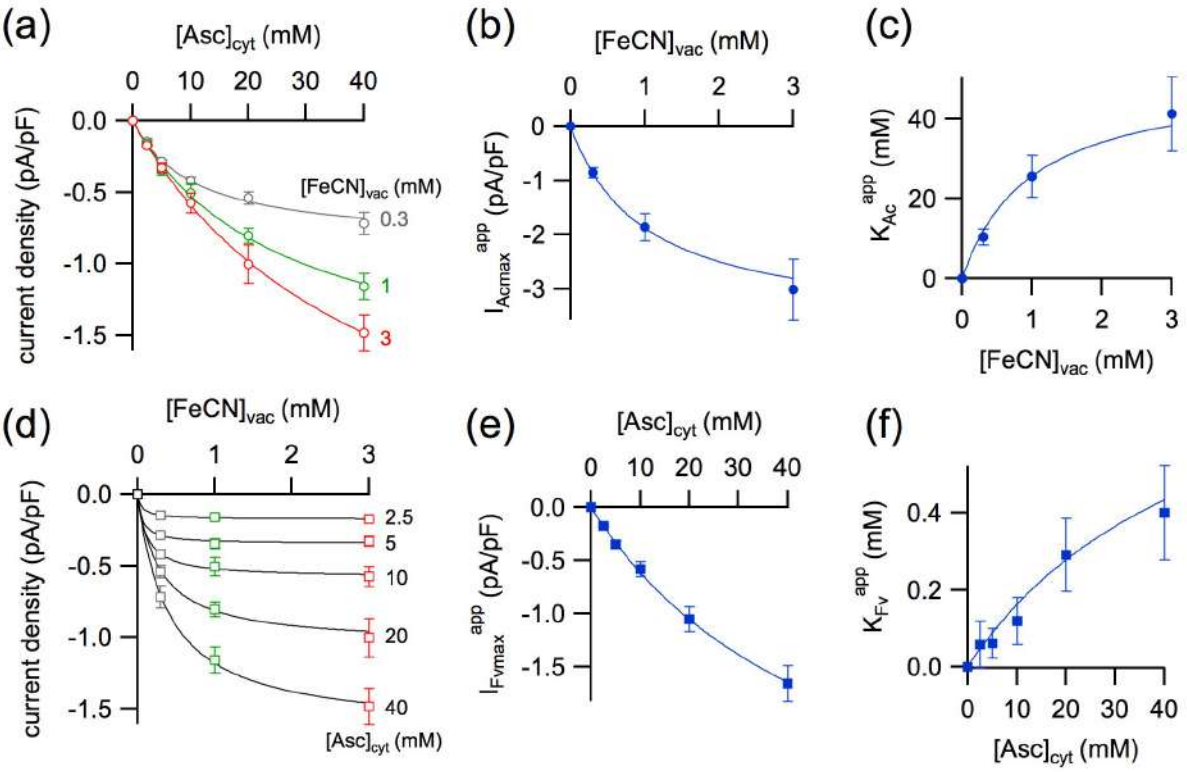

Figure 2

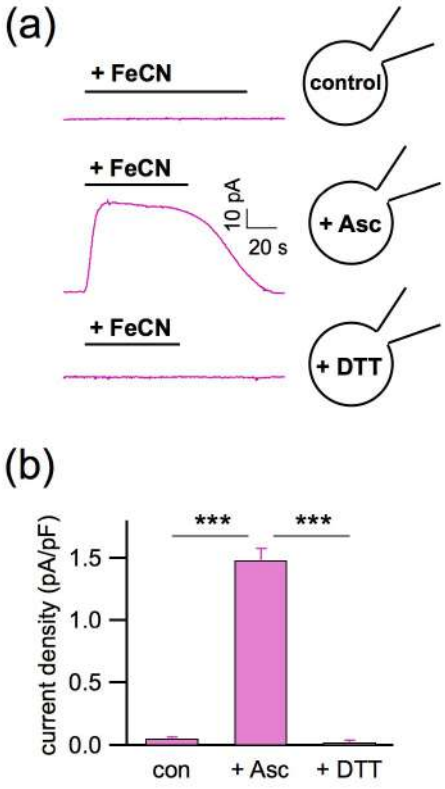

995

996 **Figure 3**

997

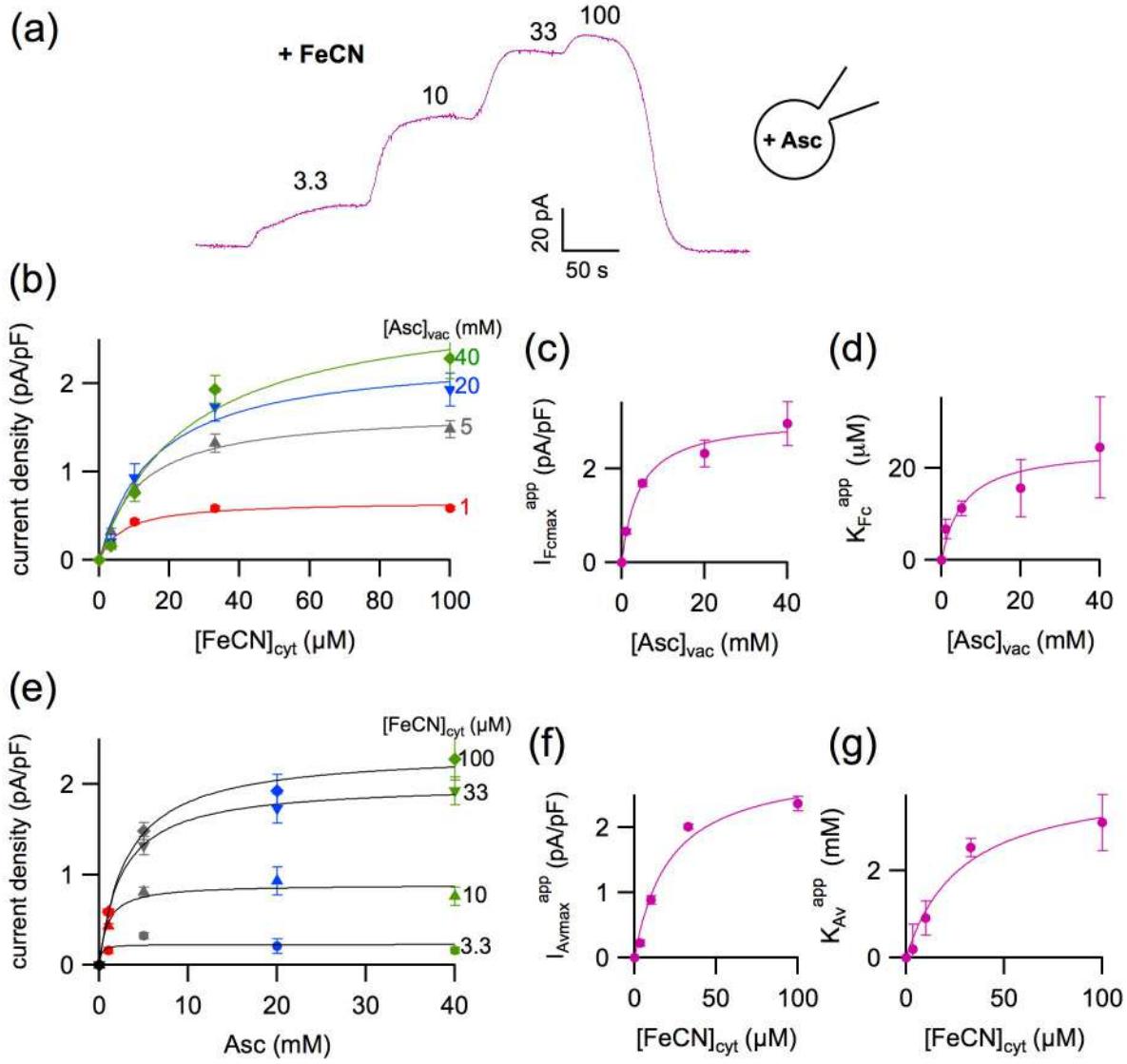
(a)
+ FeCN
3.3
10
33
100
+ Asc
20 pA
50 s
(b)
current density (pA/pF)
[Asc]vac (mM)
40
20
5
1
[FeCN]cyt (µM)
(c)
I app Fcmax (pA/pF)
[Asc]vac (mM)
(d)
K app Fc (µM)
[Asc]vac (mM)
(e)
current density (pA/pF)
[FeCN]cyt (µM)
100
33
10
3.3
Asc (mM)
(f)
I app Avmax (pA/pF)
[FeCN]cyt (µM)
(g)
K app Av (mM)
[FeCN]cyt (µM)

Figure 4

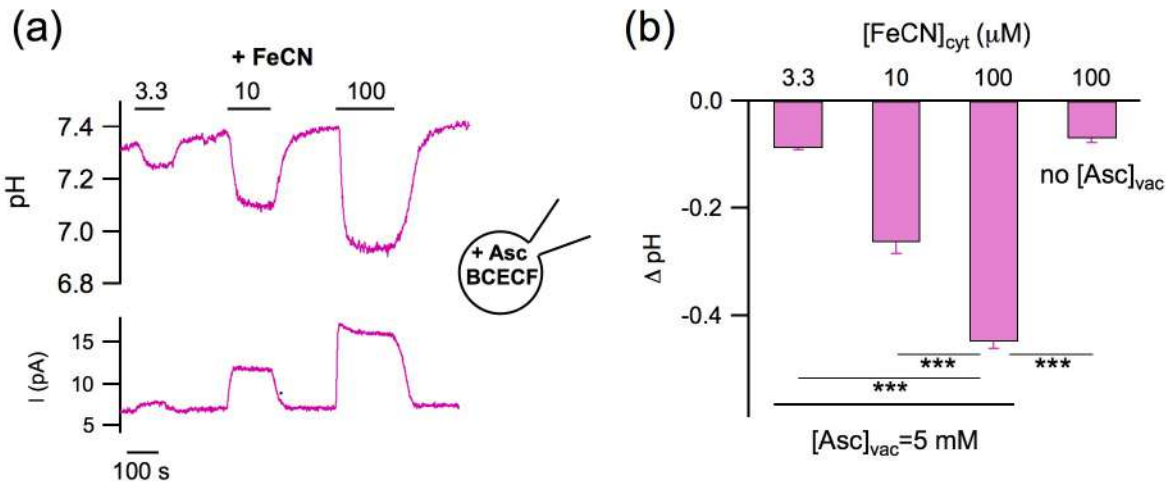

1001

1002 **Figure 5**

1003

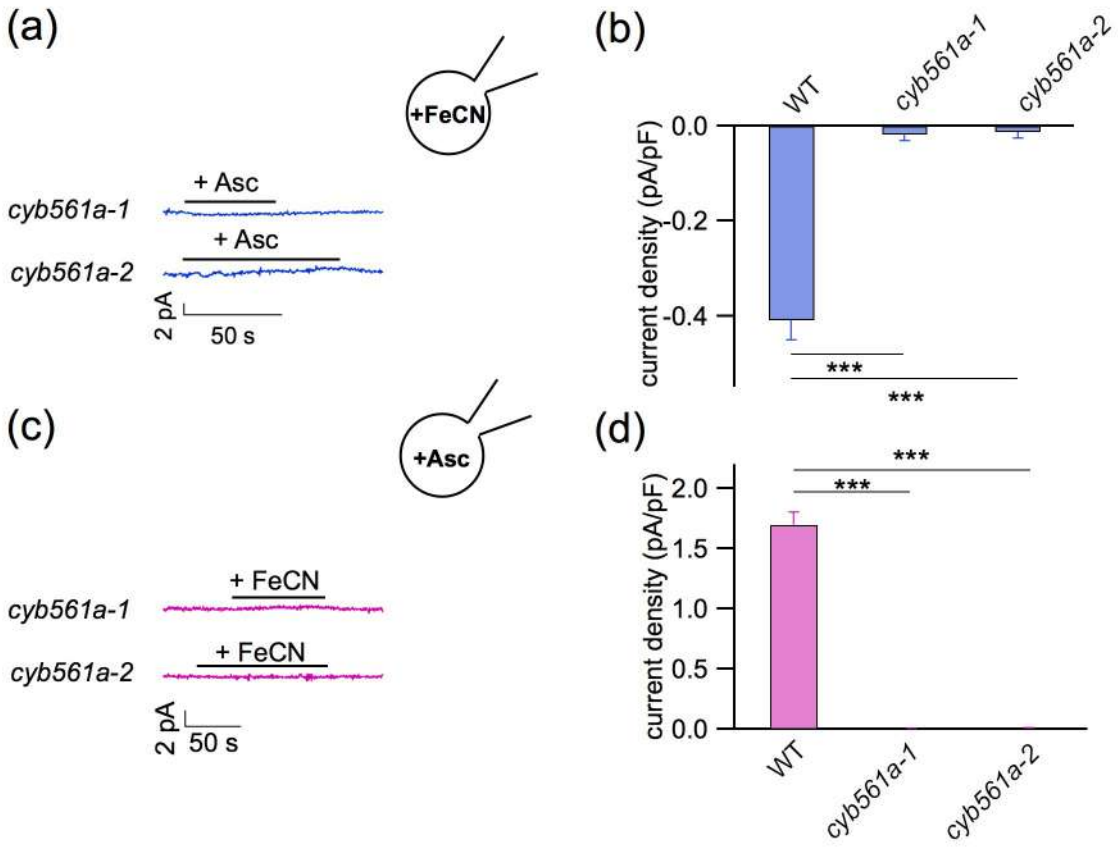

1004

1005 **Figure 6**

1006

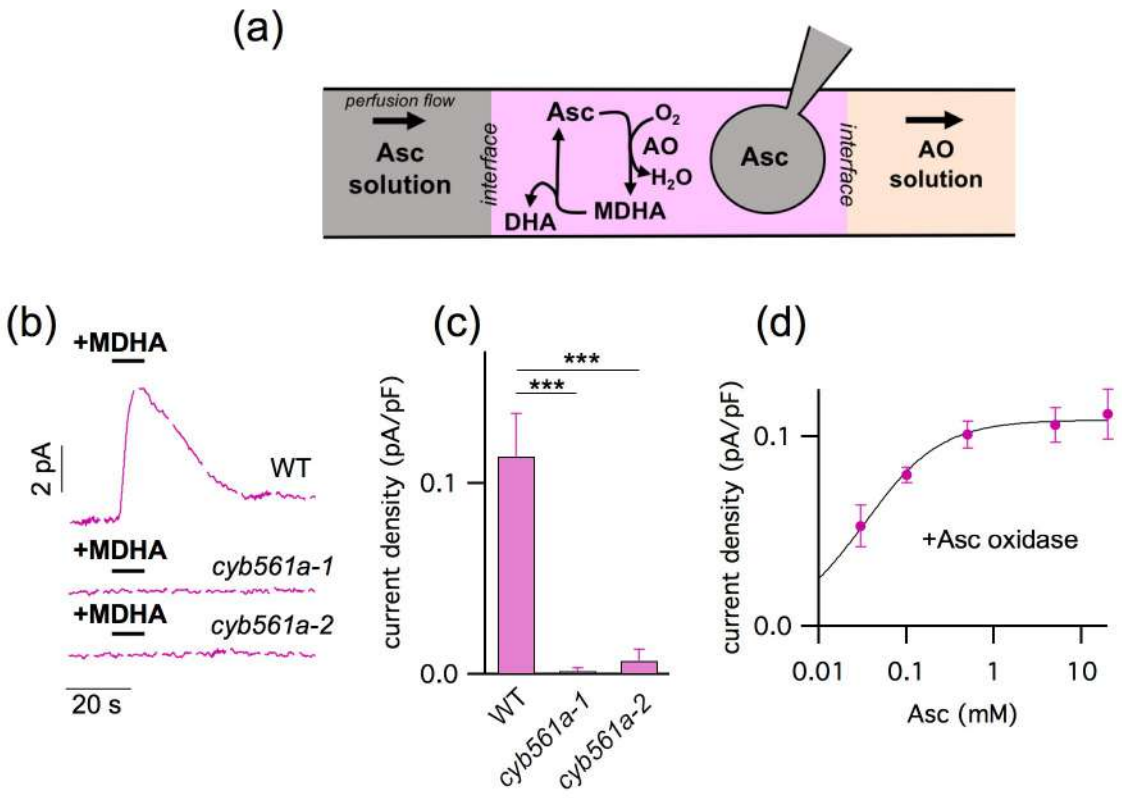

1007

1008 **Figure 7**

1009

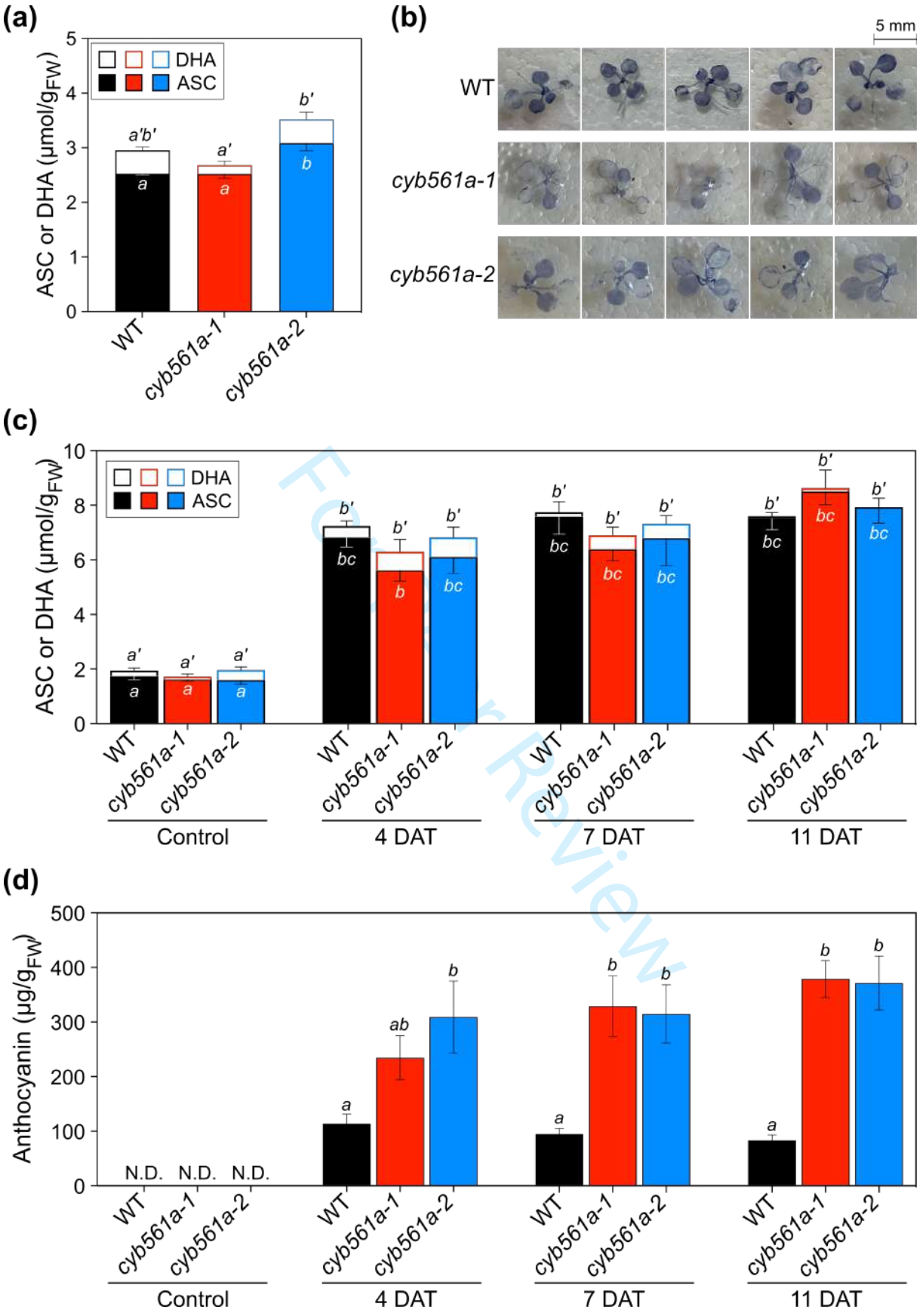
(a)
ASC or DHA (μmol/g$_{FW}$)
DHA
ASC
WT
cyb561a-1
cyb561a-2
(b)
5 mm
WT
cyb561a-1
cyb561a-2
(c)
ASC or DHA (μmol/g$_{FW}$)
DHA
ASC
Control
4 DAT
7 DAT
11 DAT
(d)
Anthocyanin (μg/g$_{FW}$)
N.D.
Control
4 DAT
7 DAT
11 DAT

Figure 8

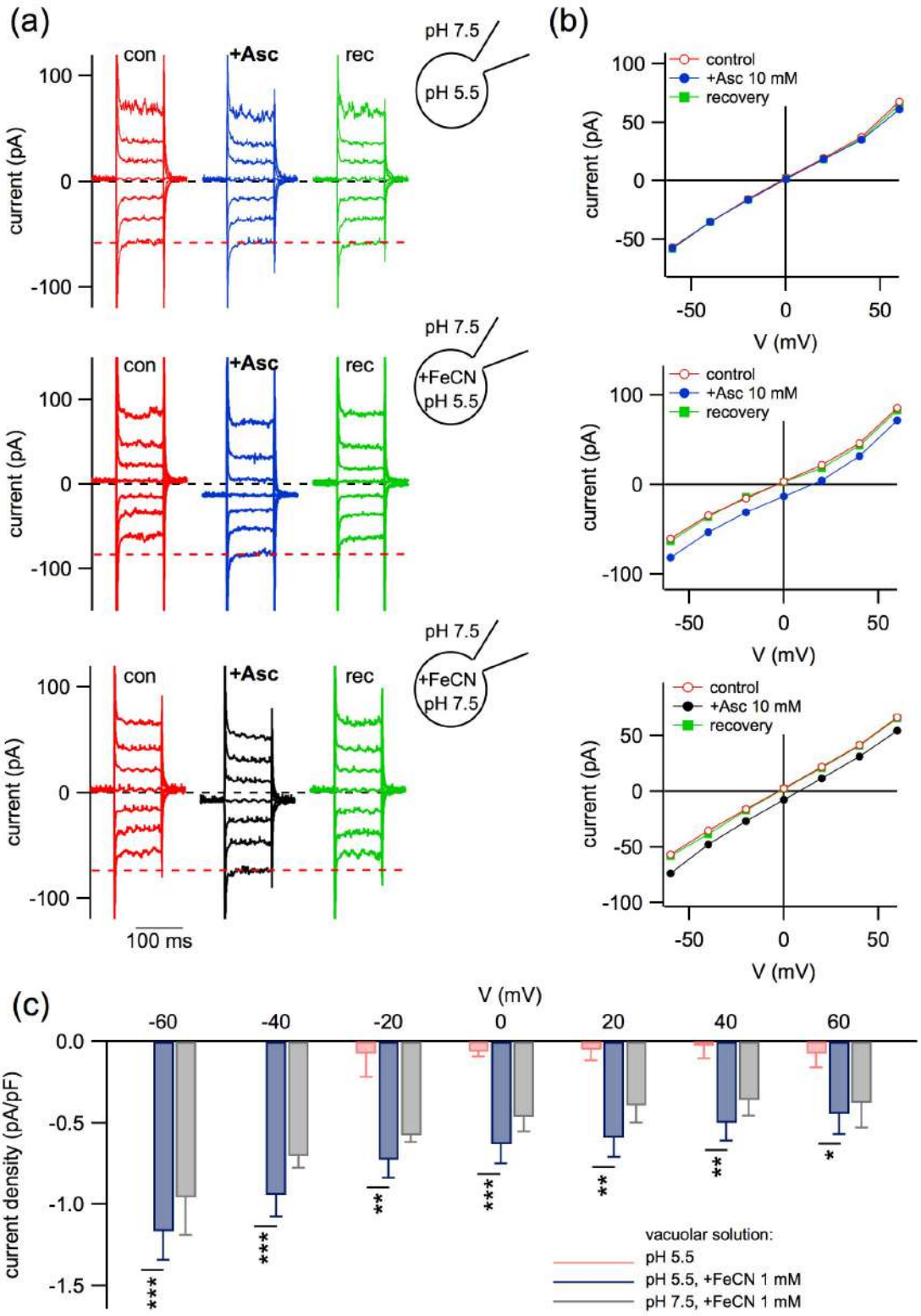

Supplemental Figure 1

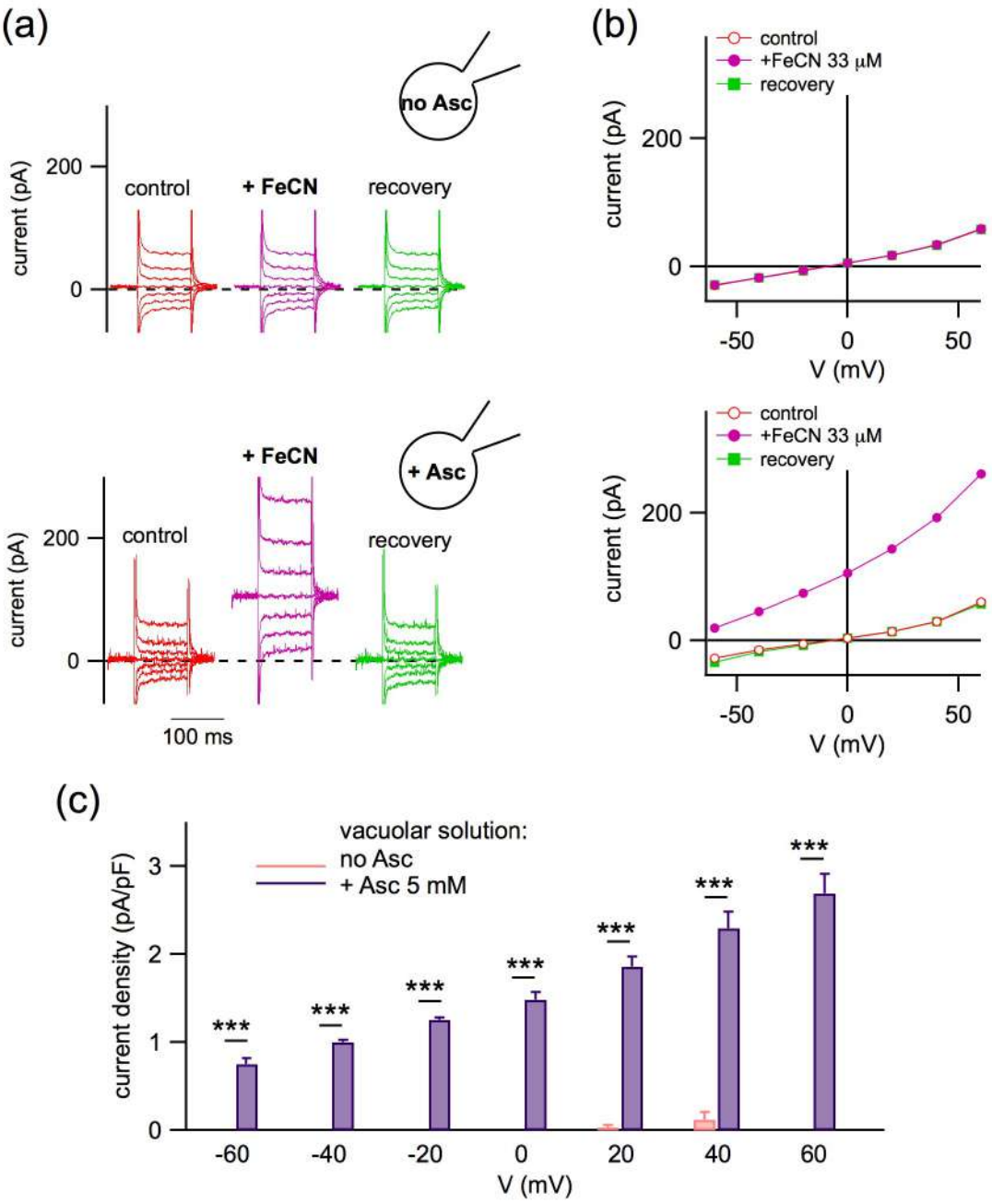

Supplemental Figure 2

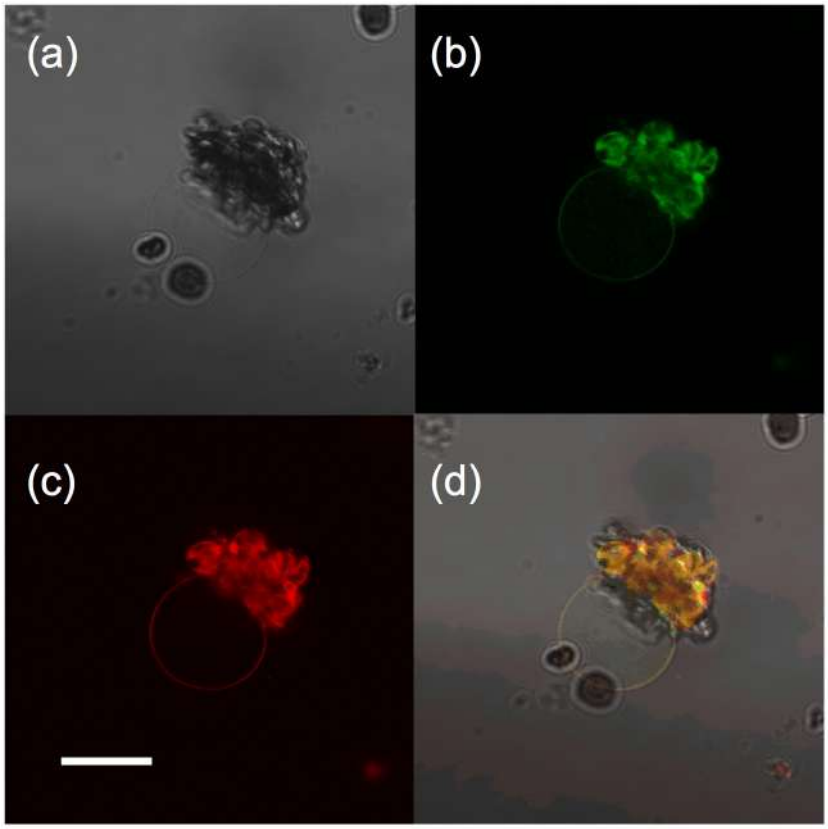

Supplemental Figure 3

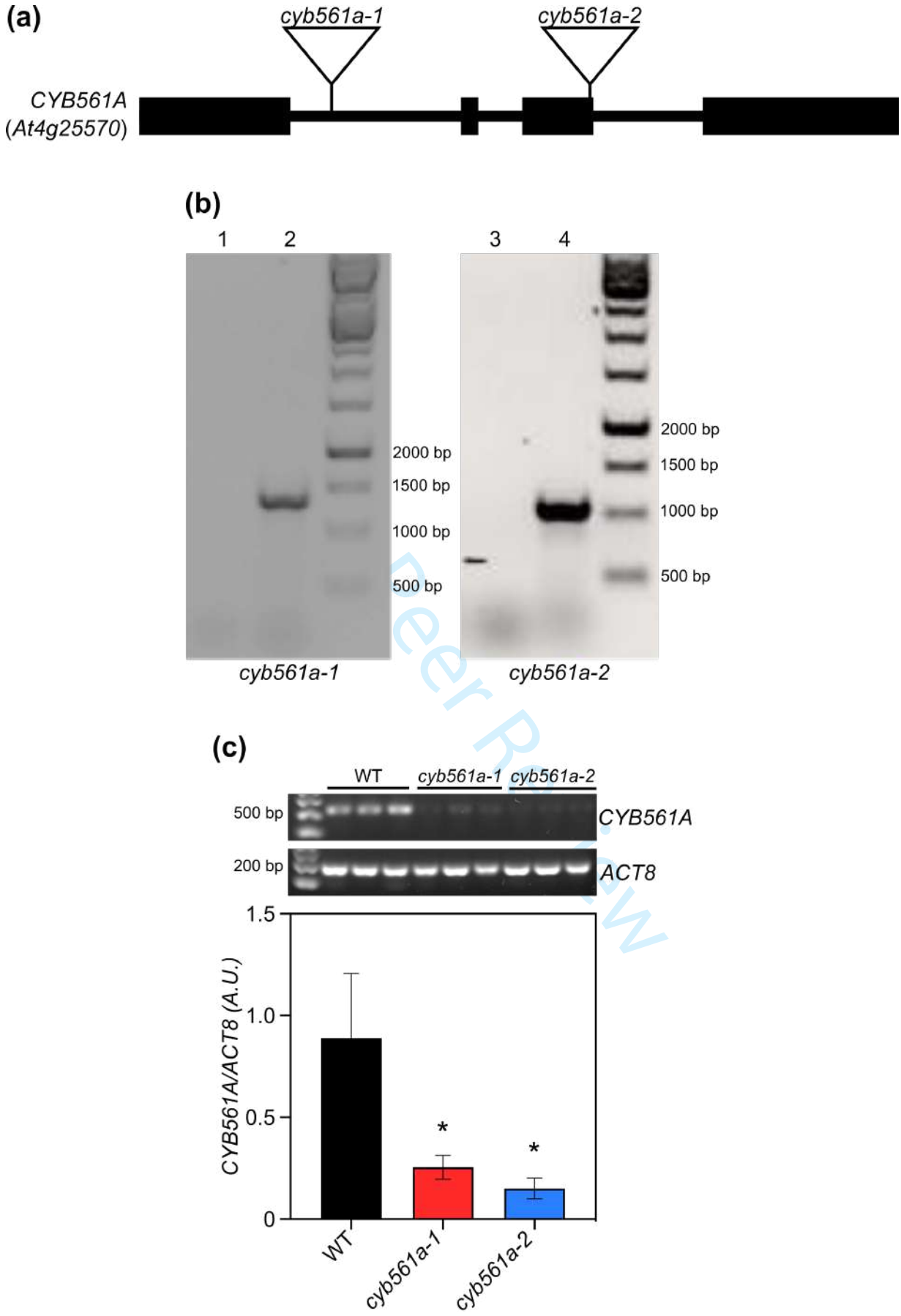

1022

1023 **Supplemental Figure 4**

1024

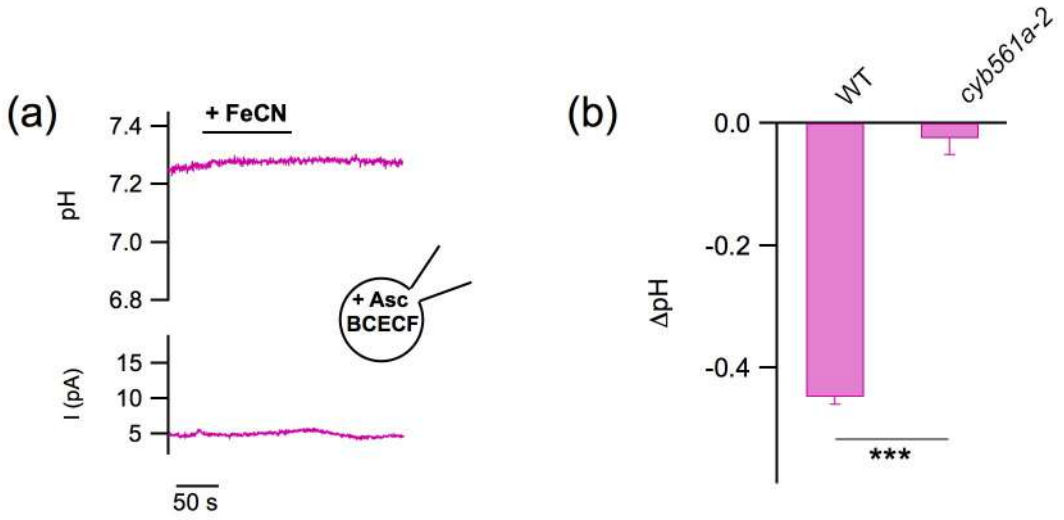

1025

1026 **Supplemental Figure 5**

1027

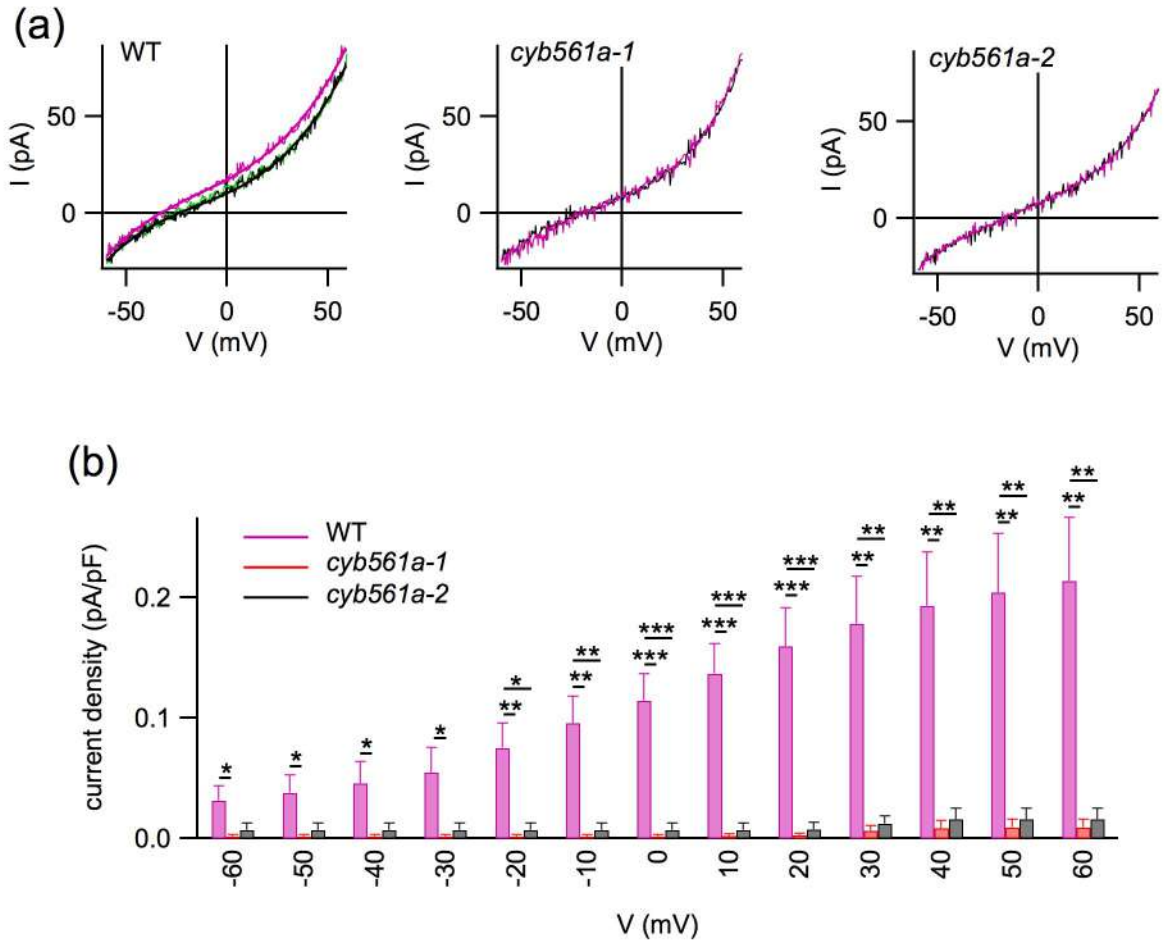

1028

1029 **Supplemental Figure 6**

1030

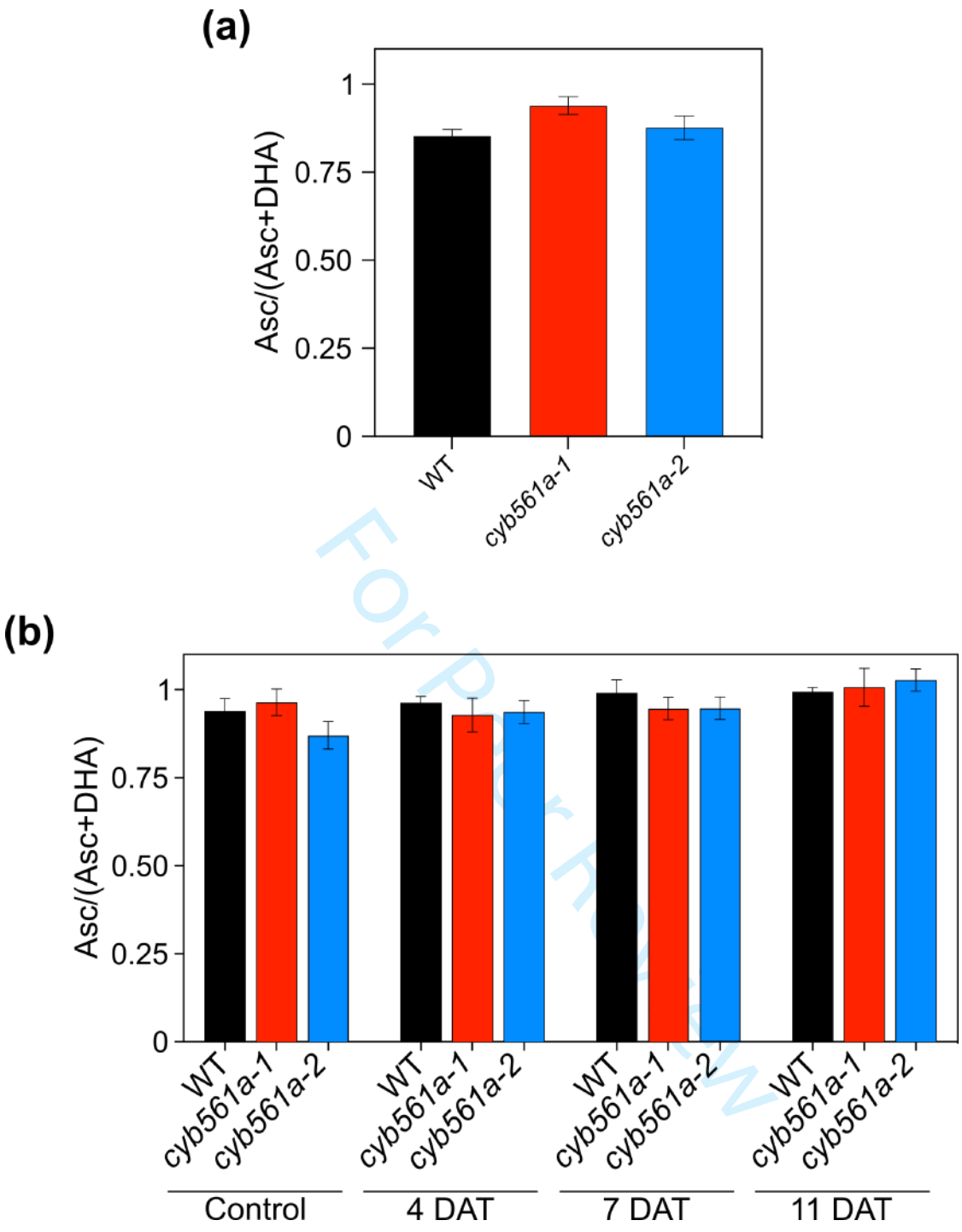

Supplemental Figure 7

WT

cyb561a-1

cyb561a-2

1034

1035 **Supplemental Figure 8**